Nucleic Acids Research, 2023, 1–22
https://doi.org/10.1093/nar/gkad1202
RNA and RNA-protein complexes

GPATCH4 regulates rRNA and snRNA 2′-*O*-methylation in both DHX15-dependent and DHX15-independent manners

Nidhi Kanwal[1], Nicolai Krogh[2], Indira Memet[1], Nicolas Lemus-Diaz[1], Chairini C. Thomé[1], Luisa M. Welp[3,4], Athanasia Mizi[5], Philipp Hackert[1], Argyris Papantonis[5], Henning Urlaub[3,4,6,7], Henrik Nielsen[2], Katherine E. Bohnsack[1,6,*] and Markus T. Bohnsack[1,6,7,8,*]

[1]Department of Molecular Biology, University Medical Center Göttingen, Humboldtallee 23, 37073 Göttingen, Germany
[2]Department of Cellular and Molecular Medicine, University of Copenhagen, 3B Blegdamsvej, 2200N Copenhagen, Denmark
[3]Max Planck Institute for Multidisciplinary Sciences, Bioanalytical Mass Spectrometry, Am Fassberg 11, 37077 Göttingen, Germany
[4]Institute for Clinical Chemistry, University Medical Center Göttingen, Robert-Koch-Straße 40, 35075 Göttingen, Germany
[5]Institute of Pathology, University Medical Center Göttingen, Robert-Koch-Straße 40, 35075 Göttingen, Germany
[6]Göttingen Center for Molecular Biosciences, Georg-August University Göttingen, Justus-von-Liebig-Weg 11, 37077 Göttingen, Germany
[7]Cluster of Excellence 'Multiscale Bioimaging: from Molecular Machines to Networks of Excitable Cells' (MBExC), University of Göttingen, Göttingen
[8]Max Planck Institute for Multidisciplinary Sciences, Am Fassberg 11, 37077 Göttingen, Germany

[*]To whom correspondence should be addressed. Tel: +49 551 3965968; Fax: +49 551 395960; Email: markus.bohnsack@med.uni-goettingen.de
Correspondence may also be addressed to Katherine E. Bohnsack. Tel: +49 551 3969305; Fax: +49 551 395960; Email: katherine.bohnsack@med.uni-goettingen.de

Abstract

Regulation of RNA helicase activity, often accomplished by protein cofactors, is essential to ensure target specificity within the complex cellular environment. The largest family of RNA helicase cofactors are the G-patch proteins, but the cognate RNA helicases and cellular functions of numerous human G-patch proteins remain elusive. Here, we discover that GPATCH4 is a stimulatory cofactor of DHX15 that interacts with the DEAH box helicase in the nucleolus via residues in its G-patch domain. We reveal that GPATCH4 associates with pre-ribosomal particles, and crosslinks to the transcribed ribosomal DNA locus and precursor ribosomal RNAs as well as binding to small nucleolar- and small Cajal body-associated RNAs that guide rRNA and snRNA modifications. Loss of GPATCH4 impairs 2′-*O*-methylation at various rRNA and snRNA sites leading to decreased protein synthesis and cell growth. We demonstrate that the regulation of 2′-*O*-methylation by GPATCH4 is both dependent on, and independent of, its interaction with DHX15. Intriguingly, the ATPase activity of DHX15 is necessary for efficient methylation of DHX15-dependent sites, suggesting a function of DHX15 in regulating snoRNA-guided 2′-*O*-methylation of rRNA that requires activation by GPATCH4. Overall, our findings extend knowledge on RNA helicase regulation by G-patch proteins and also provide important new insights into the mechanisms regulating installation of rRNA and snRNA modifications, which are essential for ribosome function and pre-mRNA splicing.

Graphical abstract

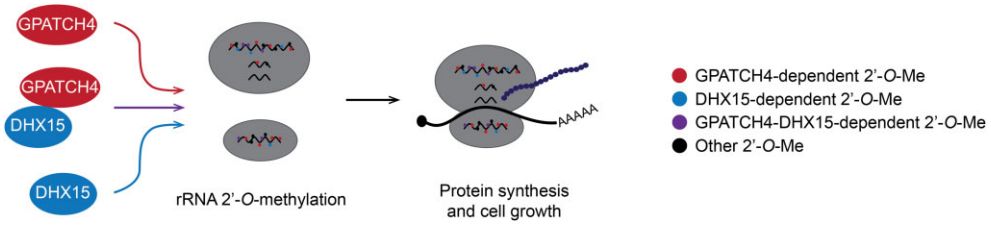

Introduction

Gene expression requires the assembly of various ribonucleoprotein (RNP) complexes, including spliceosomes that remove intronic sequences during pre-mRNA maturation and ribosomes, which are responsible for the synthesis of all cellular proteins. Eukaryotic cytosolic ribosomes are composed of small (40S) and large (60S) subunits containing four ribosomal RNAs (rRNAs; 18S, 5.8S, 28S and 5S) and approximately 80 ribosomal proteins (RPs) (1,2). Production of the ribosomal subunits is a highly dynamic and energy-consuming process involving > 200 assembly factors that associate transiently with the pre-ribosomal subunits to orchestrate rRNA modification, folding and processing, and the hierarchical recruitment of RPs (3–5). In human cells, transcription of ribosomal DNA (rDNA) by RNA polymerase I (Pol I) synthesises a precursor rRNA (pre-rRNA) transcript containing the 18S, 5.8S and 28S rRNAs separated by internal transcribed spacers (ITS1 and ITS2) and flanked by external transcribed spacers (5′ ETS and 3′ ETS). The 5S rRNA is independently synthesised by RNA polymerase III (Pol III) and incorporated into nascent pre-60S particles as a pre-assembled 5S RNP complex together with

Received: August 10, 2023. **Revised:** December 1, 2023. **Editorial Decision:** December 1, 2023. **Accepted:** December 5, 2023

the RPs uL5 and uL18 (6,7). Processing of the pre-rRNA transcript involves a series of endoribonucleolytic cleavages and exoribonucleolytic trimming steps that are carefully coordinated with recruitment and positioning of the RPs (8). Assembly of the ribosomal subunits is initiated in the nucleolus, whereas final maturation steps occur in the cytosol (3–5).

In contrast to mature ribosomes that are able to perform numerous rounds of mRNA translation, spliceosomes are assembled *de novo* on each pre-mRNA requiring intron removal. The sequential association and dissociation of small nuclear RNPs (snRNPs), composed of small nuclear RNAs (snRNAs) and associated proteins, leads to the formation of a series of spliceosomal complexes (9). The U1 snRNP marks the 5′splice site (ss) by base pairing, and the U2 snRNP similarly marks the branch site by base pairing and together with associated protein factors defines the 3′ ss. This facilitates subsequent recruitment of the U4/U6.U5 tri-snRNP. Structural rearrangements induce the release of the U1 and U4 snRNPs to form a catalytically active spliceosome that mediates intron excision before ultimately being disassembled into its constituent snRNP components. The snRNA components of the major spliceosome, with the exception of U6 (10), are synthesized by RNA polymerase II (Pol II) from snRNA genes that are often physically associated with Cajal bodies (11). Apart from U6, the snRNAs are exported to the cytosol where they undergo various maturation steps before being re-imported into the nucleoplasm where they are enriched in Cajal bodies (12).

During their biogenesis, both rRNAs and snRNAs are extensively modified by stand-alone and RNA-guided modification enzymes (13,14). Collectively, modifications in the rRNAs modulate the conformational flexibility of the rRNA scaffolds of the ribosomal subunits, enabling efficient and faithful translation. Similarly, snRNA modifications facilitate snRNP biogenesis by promoting correct snRNA folding as well as fine-tuning spliceosome function to ensure accurate splice site selection and efficient intron excision. In terms of the number of sites, the majority of rRNA and snRNA modifications are introduced by small nucleolar RNPs (snoRNPs) and small Cajal body-associated RNPs (scaRNPs), respectively (13,15). snoRNPs and scaRNPs are composed of a guide RNA and associated proteins, including a catalytic subunit and other proteins that fulfil scaffolding roles and/or contribute to maintaining the correct localization of the complexes. Box C/D sno/scaRNAs contain the 2′-*O*-ribose methyltransferase fibrillarin or the acetyltransferase NAT10 whereas the pseudouridine synthase dyskerin is present in box H/ACA sno/scaRNPs (16–18). Typically, the RNA component of the sno/scaRNP basepairs with the target RNA, positioning the catalytic subunit appropriately to allow modification of a specific target nucleotide. However, examples of non-modification-guiding snoRNAs exist and in these cases, the basepairing interactions that the snoRNAs make with the pre-rRNA contribute to regulating rRNA folding either by preventing premature basepairing of particular sequences and/or tethering specific rRNA sequences in desired conformations (see for example, (19–21)).

Ensuring sno/scaRNP access to target sites and their timely release from pre-ribosomes/snRNPs are critical to ensure efficient RNA modification and ongoing RNP biogenesis. While it is clear that sno/scaRNP association with pre-ribosomes/snRNPs is coordinated with other maturation events, little is currently known about how, on the mechanistic level, sno/scaRNP recruitment is orchestrated. However, as key remodellers of RNP complexes, NTP-dependent RNA helicases represent potential regulators of sno/scaRNP dynamics on their substrate RNPs. Indeed, numerous RNA helicases are implicated in facilitating the release of snoRNPs from pre-ribosomal particles (reviewed in (22)). For example, in yeast, changes in snoRNA levels on pre-ribosomes and defects in rRNA modification are observed when the DEAD box ATPase Dbp3 or the DEAH box helicase Prp43 are lacking (23–25).

Notably Prp43 and its human homologue DHX15 are multifunctional RNA helicases that contribute to several different aspects of gene expression (26). Beyond their roles in ribosome assembly where Prp43 is required for release of a cluster of snoRNAs from pre-60S particles (25) and DHX15 is necessary for an early pre-rRNA cleavage event (27), both Prp43 and DHX15 are involved in spliceosome disassembly and quality control (28–30), and DHX15 is also implicated in the innate immune response to viral infection (31,32). The diverse functions and targets of Prp43/DHX15 necessitate dedicated strategies to ensure recruitment of the helicases to appropriate RNAs and to ensure helicase activity only on desired substrates. This is accomplished by cofactors belonging to the G-patch protein family (33). G-patch proteins are characterised by a glycine-rich domain (34) via which they interact with cognate RNA helicases. Structural and biochemical analyses demonstrate that the G-patch domain, which comprises a N-terminal α-helix and a C-terminal disordered loop, contacts the winged-helix and RecA2 domains of cognate helicases, thereby tethering the helicase core in an optimal conformation for efficient catalysis (35,36). More than 20 G-patch proteins are expressed in human cells and the functions of some are already described. For example, the NF-κB-repressing factor (NKRF) is a cofactor of DHX15 that is required for recruitment of XRN2 to early pre-ribosomal particles (27) and, independent of its interaction with DHX15, TFIP11 is implicated in regulating U6 snRNA modification and U4/U6.U5 tri-snRNP assembly (37). However, the cellular roles and associated RNA helicases of numerous G-patch proteins remain uncharacterised.

Here, we reveal that GPATCH4 is a cofactor of DHX15 that stimulates its ATPase activity. GPATCH4 interacts with DHX15 in the nucleolus and these proteins associate with pre-ribosomal particles. Chromatin immunoprecipitation (ChIP), crosslinking and analysis of cDNA (CRAC) and RNA immunoprecipitation followed by small RNA-seq demonstrate that GPATCH4 crosslinks to rDNA and pre-rRNAs as well as binding to sno/scaRNAs. Global analysis of rRNA and snRNA 2′-*O*-methylation with RiboMeth-seq revealed that knockout of GPATCH4 impairs methylation at several sites. Using targeted 2′-*O*-methylation-sensitive RNase H-based cleavage assays, we demonstrate the importance of GPATCH4 for 2′-*O*-methylations; at some sites GPATCH4 acts independently of DHX15 while at other sites, its interaction with DHX15 is required. With respect to DHX15, we further show that its ATPase activity is necessary for efficient methylation at the DHX15-dependent sites, suggesting a potential function of DHX15 in ensuring efficient snoRNA-guided 2′-*O*-methylation of rRNA that requires activation by GPATCH4.

Materials and methods

Molecular cloning

The coding sequences (CDS) for GPATCH4 (NM_001396855.1), DHX15 (NM_001358.2) and NOLC1 (NM_004741.5) were cloned into pcDNA5 expression vector. The CDSs of GPATCH4 and NOLC1 were cloned for expression of proteins with a C-terminal 6xHis-PreScisson protease site-2xFlag (His-Flag) tag and DHX15 CDS was cloned for expression of a protein with a 2xFlag-PreScission protease site-6xHis (Flag-His) tag at the N-terminus for the generation of stable cell lines using primers listed in Supplementary Table S1. Site-directed mutagenesis was employed to generate amino acid substitution mutants of GPATCH4 and DHX15, and siRNA resistant mutants of DHX15 (Supplementary Table S1). For CRISPR/Cas9 genome editing, guide RNA sequences (Supplementary Table S1) were cloned into PX459 plasmid pSpCas9(BB)-2A-Puro (Addgene plasmid no. 62988) as described (38). For recombinant protein expression, coding sequences of DHX15 or its catalytically inactive mutant $DHX15_{E261Q}$ and $GPATCH4_{GP}$ (amino acids 11 to 57) were cloned into pQE-based expression plasmids (Supplementary Table S1). Plasmids generated in this study are listed in Supplementary Table S2.

Human cell culture, stable cell line and CRISPR/Cas9 genome editing, RNAi

HEK293 Flp-In™ T-REx™ cells were maintained in DMEM containing 10% foetal bovine serum (FBS) and 1% penicillin-streptomycin (Pen-Strep) under standard conditions (37°C and 5% CO_2). For generation of stably transfected cell lines, cells were co-transfected with the appropriate pcDNA5-based constructs and the pOG44 Flp-recombinase expression plasmid (Thermo Fisher Scientific). Cells that correctly inserted the transgene into the Flp-In locus were selected with hygromycin (100 μg/mL) and blasticidin (10 μg/mL). Expression of proteins from the transgene was induced using 1 μg/mL tetracycline for 24 h.

The GPATCH4 knockout cell line was generated using CRISPR/Cas9 technology (38). Briefly, HEK293 Flp-In™ T-REx™ cells (Supplementary Table S3) were transfected with a PX459 plasmid for expression of an appropriate guide RNA and the Cas9 nuclease (Supplementary Table S2) and selected with puromycin (1 μg/mL). Selected cells were seeded at single cell density in 96-well plates. To test genomic cleavage efficiency, the GeneArt® Genomic Cleavage Detection Kit (ThermoFisher Scientific) was used according to the manufacturer's instructions. Populations deriving from single cells were grown and genomic DNA was extracted using the PureLink Genomic DNA kit (ThermoFisher Scientific) according to the manufacturer's instructions. The extracted DNA was used to amplify the targeted region of the genome using oligonucleotides listed in Supplementary Table S1 and the amplicon was sequenced to check for genomic variations. The absence of GPATCH4 protein was monitored by western blotting using antibodies listed in Supplementary Table S4. For siRNA-mediated RNAi, cells were transfected with 50 nmol of the appropriate siRNA (siNT 5′-AGUACGCGGAAUACUUCGAdTdT-3′, siDHX15 5′-GGUUAUAGUUAUGAGCGCUACU-CUAdTdT-3′) using lipofectamine RNAiMAX (Thermo Fisher Scientific) according to the manufacturer's instructions and were harvested 96 h after transfection.

Immunofluorescence

Cells were grown on coverslips coated with 0.01% (v/v) poly-L-lysine and fixed with 4% paraformaldehyde (PFA) for 15 min at room temperature (RT). Cells were permeabilised with 0.1% (v/v) Triton X-100 in 1XPBS (phosphate buffered saline- 137 mM NaCl, 2.7 mM KCl, 10 mM Na_2HPO_4 and 1.8 mM KH_2PO_4) followed by blocking with 10% FBS for 1 h at RT. Incubation with primary antibodies (Supplementary Table S4) was performed for 2 h at RT (39). Following washes with 1XPBS, incubation with Alexa Fluor 488-, 594- or 647-conjugated secondary antibodies was performed for 1 h at RT. Coverslips were mounted onto slides using VECTASHIELD mounting medium supplemented with 4′,6-diamidino-2-phenylindole (DAPI) and fluorescence intensity was detected using ZEISS LSM500 confocal microscope at 100X objective. The acquired images were analysed and processed using Fiji software.

Nucleolar extract preparation

Nuclei were separated on a sucrose cushion as previously described in (27) with slight modifications. Approximately 80×10^6 cells were lysed using Dounce homogeniser in 5 ml of ice-cold lysis buffer (20 mM Tris–HCl pH 7.4, 10 mM KCl, 3 mM $MgCl_2$, 0.1% (v/v) NP-40 and 10% (v/v) glycerol) and nuclei were pelleted by centrifugation at 1350 g for 10 min. The supernatant was retained as the cytosolic fraction. The pellet was resuspended in sucrose solution S1 (0.25 M sucrose and 10 mM $MgCl_2$), layered on top of 3 ml of solution S2 (0.35 M sucrose and 0.5 mM $MgCl_2$) and centrifuged at 1430 g for 5 min. The pellet was resuspended in 3 ml of sucrose solution S2, sonicated for 6 cycles at 20% amplitude (10 sec on, 10 sec off) to release nucleoli and layered on top of 3 ml sucrose solution S3 (0.88 M sucrose and 0.5 mM $MgCl_2$) and centrifuged at 3000 g for 10 min. The upper phase was retained as nucleoplasmic fraction and the nucleolar pellet was incubated on ice for 30 min in 400 μl high-salt buffer (20 mM HEPES–NaOH pH 8.0, 500 mM KCl, 0.5 mM ethylenediaminetetraacetic acid (EDTA), 0.8% (v/v) Triton X-100 and 0.4% (v/v) CHAPS) supplemented with 16 U TURBO DNase (Thermo Fisher Scientific), and disrupted by sonication. Samples were then diluted four-fold with a buffer containing 20 mM HEPES–NaOH pH 8.0, 2 mM $MgCl_2$ and 13.3% (v/v) glycerol. 10 μg of protein each from total, cytosolic, nuclear, nucleoplasmic and nucleolar fractions were analysed for purity by western blotting before carrying out immunoprecipitations with anti-FLAG M2 magnetic beads (Millipore M8823) as described below.

Anti-FLAG immunoprecipitation (IP)

Stably transfected HEK293 cell lines expressing His-FLAG-/FLAG-His-tagged proteins or the His-FLAG tag were lysed by sonication in IP buffer (50 mM Tris–HCl pH 7.4, 150 mM NaCl, 0.5 mM ethylenediaminetetraacetic acid (EDTA), 0.1% (v/v) Triton-X-100, 10% (v/v) glycerol) supplemented with 1× Roche cOmplete protease inhibitor. After centrifugation, the clarified lysate was added to anti-FLAG M2 magnetic beads that had been pre-equilibrated in IP buffer and incubated for 2 h at 4°C. The beads were then washed five times with IP buffer, then FLAG-tagged

and associated proteins were eluted with 250 μg/ml of 3× FLAG peptide (Millipore F3290). Proteins in the eluate were precipitated with 20% (v/v) trichloroacetic acid (TCA) and analysed by western blotting using antibodies listed in Supplementary Table S4. In case of IPs from nucleolar extracts, the isolated nucleolar fraction was incubated with anti-FLAG M2 magnetic beads and all other steps were performed as described above.

Sucrose density gradient centrifugation

HEK293 cells were lysed by sonication in a buffer containing 50 mM Tris–HCl pH 7.4, 100 mM NaCl, 5 mM $MgCl_2$ and 1 mM dithiothreitol (DTT). Where required, cells were treated with indicated siRNAs for 96 hours or in case of GPATCH4-His-FLAG, expression of the protein was induced with 1 μg/ml tetracycline for 24 h before lysis. The clarified lysate was loaded on top of a 10–45% (w/v) sucrose gradient and (pre-)ribosomal complexes were separated by centrifugation at 23 500 rpm in an SW-40Ti rotor for 16 h at 4°C (40). Fractions were collected using a Biocomp fractionator and the absorbance at 254 nm was continuously monitored. Proteins in the fractions were precipitated with 20% (tricholoracetic acid) TCA and analysed by western blotting using antibodies given in Supplementary Table S4. Signal intensities corresponding to specific proteins in each fraction were quantified using Image Studio Lite (version 5.2.5) software. After normalisation to the input samples, the maximum signal intensity for each gradient was set to 1 and all other values adjusted accordingly to allow for comparison between different experiments. Alternatively, RNAs extracted from each fraction using TRI reagent (Sigma-Aldrich) were separated by denaturing agarose gel electrophoresis and analysed by northern blotting using probes listed in Supplementary Table S5.

Recombinant protein expression in *Escherichia coli*

Escherichia coli BL21 CodonPlus cells transformed with plasmids for the expression of MBP-DHX15-His_{10}, MBP-$DHX15_{E261Q}$-His_{10}, or ZZ-$GPATCH4_{GP}$-His_7 were grown until OD_{600} = 0.6. Expression of MBP-DHX15-His_{10} or MBP-$DHX15_{E261Q}$-His_{10} was induced with 1 mM isopropyl β-D-1-thiogalactopyranoside (IPTG) for 16 h at 18°C. In the case of ZZ-$GPATCH4_{GP}$-His_7, induction was carried out at 37°C for 3 h. The cells were pelleted and resuspend in Lysis Buffer (50 mM Tris–HCl pH 7.4, 600 mM NaCl, 1 mM $MgCl_2$, 0.5% (v/v) Triton X-100, 10% (v/v) glycerol, 25 mM imidazole and 2 mM β-mercaptoethanol). After sonication, the lysate was clarified by centrifugation at 50 000g for 30 min at 4°C. The clarified lysate was incubated with pre-equilibrated cOmplete His-tag purification resin (Roche) for 2 h at 4°C. The beads were then washed once with Wash Buffer 1 (50 mM Tris–HCl pH 7.4, 150 mM NaCl, 1 mM $MgCl_2$, 10% (v/v) glycerol and 40 mM imidazole) followed by a high-salt wash with Wash Buffer 2 (50 mM Tris–HCl pH 7.4, 1 M NaCl, 1 mM $MgCl_2$, 10% (v/v) glycerol and 40 mM imidazole), and then again with Wash Buffer 1. Elution was performed with Wash Buffer 1 supplemented with 250 mM imidazole and dialysed against the dialysis buffer (50 mM Tris–HCl pH 7.4, 150 mM NaCl,1.5 mM $MgCl_2$ and 10% (v/v) glycerol).

In vitro protein–protein binding assay

For the *in vitro* binding assay, 100 pmol of ZZ-$GPATCH4_{GP}$-His_7 was bound to IgG sepharose (GE Healthcare) that had been pre-equilibrated in 50 mM Tris–HCl pH 7.4, 100 mM NaCl, 1.5 mM $MgCl_2$, 0.05% (v/v) NP-40 and 1 mM DTT. The beads were thoroughly washed, and 100 pmol of MBP-DHX15-His_{10} was added to the ZZ-$GPATCH4_{GP}$-His_7-bound beads, and empty IgG sepharose as a control, for 1 h rotating at 4°C. Elution was carried out by adding 1X loading dye (80 mM Tris–HCl pH 6.8, 2% (v/v) sodium dodecyl sulphate (SDS), 10% (v/v) glycerol, 1.25% (v/v) β-mercaptoethanol, 12.5 mM EDTA, 0.01% (w/v) bromophenol blue) to the beads at 95°C for 10 min and the samples were analysed by western blotting using an anti-His antibody (Supplementary Table S4).

ATPase assay

The ATP hydrolysis activity of proteins was determined using an indirect NADH-coupled photometric assay as described in (41). Reactions were carried out in a buffer containing 45 mM Tris–HCl pH 7.4, 25 mM NaCl, 2 mM $MgCl_2$, 1.5 mM phosphoenolpyruvate, 300 μM NADH, 20 U/ml pyruvate kinase/lactic dehydrogenase (Sigma-Aldrich) and 4 mM ATP supplemented with 250 nM RNA helicase (MBP-DHX15-His_{10} or MBP-$DHX15_{E261Q}$-His_{10}) or the above buffer as a negative control. The reactions were further supplemented with 2 μM $polyU_{32}$ RNA substrate and/or 1.5 μM of ZZ-$GPATCH4_{GP}$-His_7 domain where indicated. The decrease in absorbance of NADH was monitored at 340 nm every 50 sec in a Thermo Fisher Scientific Appliskan multimode microplate reader and the ATPase rate was calculated using

$$ATPase\ rate\left(nM\ ATP\ hydrolysed/sec\right) = \frac{-\frac{dA340\left[\frac{OD}{sec}\right]}{dt}}{Kpath} \times 1000000$$

Kpath is the molar absorption coefficient for NADH for a given optical length, which is experimentally determined to account for background NADH decomposition.

Chromatin immunoprecipitation sequencing (ChIP-seq)

Stably transfected HEK293 cell lines for the expression of FLAG-tagged protein or the FLAG tag were treated with 1 μg/ml tetracycline for 24 h before crosslinking with 1.5 mM ethylene glycol bis-succinimidyl succinate (EGS, Thermo Fisher Scientific) for 10 min at room temperature, then with 1% PFA for 45 min at 4°C. ChIP was performed using the ChIP-IT High Sensitivity kit (Active Motif) according to the manufacturer's instructions. In brief, after quenching with 125 mM glycine, the cells were harvested in Chromatin Prep Buffer supplied with the kit and cell membranes were disrupted using a Dounce homogenizer (40 strokes). Chromatin shearing to 200–500 bp fragments was performed by sonication in Diagenode Bioruptor® Pico device (30 cycles, 30 s on, 30 s off). For each sample, 30 μg of sheared chromatin was subjected to immunoprecipitation by incubating with anti-FLAG M2 magnetic beads rotating overnight at 4°C. The beads were equilibrated and washed according to manufacturer's instructions. Elution was carried out with 250 μg/ml of 3X FLAG peptide in 1X TBS (50 mM Tris–HCl pH 7.4 and 150 mM NaCl) for 2 h at

4°C. The eluate was treated with 1 μg of Proteinase K (Roche) at 68°C overnight. After DNA purification, qPCR was performed for verification of the quality of the enriched ChIP DNA. After qPCR validation, the ChIP DNA was used to generate libraries using the TruSeq ChIP Library Preparation Kit (Illumina). Next generation sequencing was performed in a HiSeq4000 platform (Illumina) to obtain 15–20 million reads (max. sequencing read length 101 bp) from each sample and its respective input. The quality of sequencing reads was assessed using the FASTQC (version 0.11.9). Single and paired-end reads were aligned to human rDNA (accession number U13369.1) using bowtie2 (version 2.3.5.1). Duplicated reads were marked with Picard (version 3.0.0) and removed with samtools (v1.10) together with unmapped, non-primary alignment and low-quality reads (-F 1804 -q 30, respectively). The *.bam* files were converted to normalized (reads per million) *.bigwig* files using bedtools (version 2.27.1) and bedGraphToBigWig (version 4).

Crosslinking and analysis of cDNA (CRAC)

HEK293 cell lines for the expression of the His-FLAG tag or GPATCH4-His-FLAG were treated for 24 h with 1 μg/ml tetracycline. Cells were then crosslinked using UV light at 254 nm with an intensity of 2400 mJ/cm^2 (42,43). Cells were harvested and lysed by sonication in TNM150 buffer (50 mM Tris–HCl pH 7.8, 150 mM NaCl, 1.5 mM $MgCl_2$, 0.1% (v/v) NP-40 and 5 mM β-mercaptoethanol). The clarified lysates were incubated with pre-equilibrated anti-FLAG M2 magnetic beads and incubated for 2 h at 4°C, followed by washes with TNM150 and TNM1000 (50 mM Tris–HCl pH 7.8, 1 M NaCl, 1.5 mM $MgCl_2$, 0.1% (v/v) NP-40 and 5 mM β-mercaptoethanol). Elution was carried out overnight rotating at 4°C with 250 μg/ml 1× FLAG peptide diluted in TNM150. The eluates were treated with 0.1 U RNace-It Ribonuclease Cocktail (Agilent) for 30 sec at 37°C. The samples were then supplemented with 6 M guanidine hydrochloride, 300 mM NaCl and 10 mM imidazole, and incubated with 50 μl Ni-NTA beads (Qiagen) that had been pre-equilibrated with WB1 (50 mM Tris–HCl pH 7.8, 300 mM NaCl, 0.1% (v/v) NP-40, 6 M guanidine hydrochloride, 10 mM imidazole and 5 mM β-mercaptoethanol). After binding for 2 h at 4°C, the beads were washed with WB1 and PNK buffers (50 mM Tris–HCl pH 7.8, 10 mM $MgCl_2$, 0.5% (v/v) NP-40 and 5 mM β-mercaptoethanol). After dephosphorylation by TSAP (Promega), the 5′ ends of co-purified RNA fragments were labelled with [^{32}P] and sequencing adaptors (5′ adaptor: 5′-InvddTGTTCAGAGTTCTACAGTCCGACGATCNNNNNAGC-3′; 3′ adaptor: 5′-rAppTGGAATTCTCGGGTGCCAAGGddC-3′) were ligated to the 5′ and 3′ ends. The crosslinked protein-RNA complexes were eluted in WB2 (50 mM Tris–HCl pH 7.8, 50 mM NaCl, 10 mM imidazole, 0.1% (V/V) NP-40 and 5 mM β-mercaptoethanol) supplemented with 150 mM imidazole. The eluates were concentrated by TCA precipitation and separated on 4–12% NuPAGE Bis-Tris gels (Thermo Fisher Scientific) using MES buffer and transferred onto a Hybond-C membrane (GE Healthcare). Following autoradiography, the desired regions of the membrane were excised and RNA fragments were released by Proteinase K treatment. The isolated RNA was reverse transcribed using SuperScript III Reverse Transcriptase (Thermo Fisher Scientific) and PCR amplification of the resulting cDNA was done with the LA Taq DNA polymerase (TaKaRa). The resultant cDNA libraries were purified using the MinElute Gel Extraction Kit (Qiagen) according to manufacturer's recommendations. The concentration of the cDNA libraries was determined using a Qubit fluorometer (Thermo Fisher Scientific) and next-generation sequencing was performed at the NGS Integrative Genomics Core Unit (University Medical Center Göttingen) on a HiSeq 2500 system (Illumina).

The quality of fastq files was checked using FASTQC (version 0.11.0). For barcode and adaptor removal, pyBarcode Filter (version 1.4.5) and Flexbar (version 3.5.0), respectively, were used with the following arguments (pyBarcodeFilter.py -f -b barcode and flexbar - '-r',, '-t', '-q', 'TAIL', '-qf', u'i1.8′, '-qt', '13′, '-u', '0′, '-m', '21′, '-n', '8′, '-at', 'RIGHT', '-z', 'GZ', '-o', '-ao', '2′, '-ae', '0.1′, '-as'). PCR duplicates were collapsed using pyFastqDuplicateRemover (version 1.4.5) (pyFastqDuplicateRemover.py -f -o). The resulting sequencing reads were aligned to the human genome (GRCh38.12 p.29), and to the complete human rDNA repeating unit (Genbank acc. no. U13369, version GI:555853), which was modified according to (37), using STAR (version 2.7.0d) with the following arguments: –alignEndsType EndToEnd –outFilterMismatchNoverLmax 0.3 –outFilterMultimapScoreRange 10 –outReadsUnmapped Fastx –outSAMtype BAM SortedByCoordinate –outFilterMultimapNmax 60 –outSAMunmapped Within –outFilterScoreMinOverLread 0 –outFilterMatchNminOverLread 0 –outFilterMatchNmin 15 –alignSJDBoverhangMin 1000 –alignIntronMax 1

Bam files were index using IGVtools (version 2.5.3) and peak calling was performed using PEAKachu (version 0.2.0) in adaptive mode with default parameters and without normalisation option.

The count matrix of peaks was loaded into R (version 4.1.2), size factor and statistical analysis were performed using the DESeq2 (version 1.34.0) package, including batch and conditions (GPATCH4-FLAG and FLAG) in the design matrix. For differential enrichment analysis (GPATCH4-FLAG vs. FLAG) a one-tail test was used, and peaks with a p.adjust value < 0.05 and $\log_2$(Fold change) >2 were considered significantly enriched peaks. The corresponding genomic regions were then export as a bed file. Original bam files were filtered using the aforementioned bed file. Filtered bam files were analysed for genomic features using featureCounts (version 2.0.0) accounting for multimappers using the following arguments: -s 1 -T 8 -O -M -t gene -g gene_id –largestOverlap –minOverlap 5 –fraction using the small RNA GTF files derived from tRNAdb (version 17) for tRNAs, miRbase (version 20) for miRNAs, Ensemble (version 94) for snRNAs and snoDB (version 1.21) complemented with rDNA annotations. The resulting feature matrices were analysed using R custom scripts. For plotting results, batch correction was performed with the limma package (version 3.50.3) using the same design matrix from DESeq2.

RNA-immunoprecipitation (RIP)

Stably transfected HEK293 cell lines treated with 1 μg/ml tetracycline for 24 h to induce the expression of FLAG-tagged proteins. The cells were washed with 1X PBS and crosslinked with UV (254 nm) 3X at 800 mJ/cm^2 using a Stratalinker (Stratagene). The cells were lysed in RIP buffer (20 mM HEPES–NaOH pH 7.5, 250 mM NaCl, 1 mM $MgCl_2$,

0.5% Triton X-100 and 10% (v/v) glycerol) supplemented with cOmplete Mini Protease Inhibitor Cocktail (Roche) and 80 U RNasin Ribonuclease Inhibitor (Promega). Protein–RNA complexes were immunoprecipitated using anti-FLAG M2 magnetic beads for 3 h at 4°C and eluted with 250 μg/ml 3× FLAG Peptide for 1 h at 4°C. The eluate was treated with 2 U TURBO DNase for 20 min at 37°C in the presence of 40 U RiboLock RNase Inhibitor (Thermo Fisher Scientific). To digest proteins, the samples were incubated with 275 μg/ml Proteinase K in the presence of 1% (v/v) SDS and 0.5 mM EDTA for 2 h at 42°C in a reaction. RNAs present in the input and eluate samples were extracted using phenol:chloroform:isoamylalcohol (PCI: 25:24:1) using standard methods. Recovered RNAs were either analysed by northern blotting or small RNA-seq.

Small RNA-seq

Small RNAs <200 nt were enriched and libraries were constructed using the QIAseq miRNA Library Kit (Qiagen) according to the manufacturer's instructions and sequencing was performed on an Illumina HiSeq 4000 system at the NGS Integrative Genomics Core Unit (University Medical Center Göttingen). Fastq files were checked using FASTQC (v0.11.0) quality filtering and 3′ adaptors were trimmed using Flexbar (version 3.5.0) with the following arguments (-qf i1.8 -qt 13 -u 0 -m 15 -n 8 -at RIGHT -z GZ -o -ao 2 -ae 0.1 -as AACTGTAGGCACCATCAAT). Compressed filtered fastq files were aligned to the human genome (GRCh38.12 p.29) using STAR (version 2.7.10a) with the following arguments:–alignEndsType EndToEnd –outFilterMismatchNmax 10 –outFilterMultimapScoreRange 10 –quantMode TranscriptomeSAM GeneCounts –outReadsUnmapped Fastx –outSAMtype BAM SortedByCoordinate –outFilterMultimapNmax 30 –outSAMunmapped Within –outFilterScoreMinOverLread 0 –outFilterMatchNminOverLread 0 –outFilterMatchNmin 16 –alignSJDBoverhangMin 1000 –alignIntronMax 1 –readFilesCommand zcat. Bam files were index using IGVtools (version 2.5.3) and reads were assigned to genomic features using featureCounts (version 2.0.0) accounting for multimappers using the arguments: -s 1 -T 8 -O -M -t gene -g gene_id –largestOverlap –fraction –minOverlap 5. The gencode GTF file version 108 and the small RNA GTF files derived from tRNAdb (version 17) for tRNAs, miRbase (version 20) for miRNAs, Ensemble (version 94) for snRNAs and snoDB (version 1.21) for sno/scaRNA were used.

The output of the genomic feature matrices was analysed using R (version 4.1.2) and DEseq2 (version 1.34.0). Differential enrichment was performed after normalization by library size, using a one-tail test with an LFC threshold >0. Genes with a *P*.adjust value <0.05 were considered to encode significantly enriched transcripts. Plots were generated in R using custom-made scripts.

snoRNA and pre-rRNA analysis by northern blotting

Eluates form RIP were mixed with 2× RNA loading dye (80% (v/v) formamide, 1 mM EDTA, 0.025% (w/v) bromophenol blue, 0.025% (w/v) xylene cyanol) and separated on a 12% denaturing (7M urea) polyacrylamide gel and transferred to Hybond N+ membrane by electroblotting in 0.5XTBE (45 mM Tris, 45 mM boric acid and 1 mM EDTA). Alternatively, 5 μg of total RNA extracted using TRI reagent (Sigma-Aldrich) was denatured in 5 volumes of glyoxal loading dye and separated on a 1.2% agarose gel and transferred to Hybond N + membrane by vacuum blotting in 6× saline-sodium citrate (SSC) buffer (0.9 M NaCl and 90 mM trisodium citrate). In both cases, the RNA samples were crosslinked to the membrane by irradiating 2× with UV light at 254 nm at 120 mJ/cm^2 in a Stratalinker. Membranes were pre-hybridized in SES1 (0.25 M sodium phosphate pH 7.0, 7% (w/v) SDS and 1mM EDTA) buffer for 30 min and incubated with 5′ [^{32}P]-labelled DNA oligonucleotides (Supplementary Table S5) in SES1 buffer at 37°C overnight. After two washing steps with 6× SSC, and 2× SSC supplemented with 0.1% (w/v) SDS for 30 min each at 37°C, the membranes were exposed to a phosphorimager screen and signals were detected using a Typhoon FLA9500 (Cytiva). The acquired images were analysed and quantified using the Image StudioLite 5.2.5 software (LI-COR).

Crosslinking mass spectrometry for mapping RNA-protein contacts

A stably transfected HEK293 cell line for the expression of GPATCH4-His-FLAG was treated for 24 h with 1 μg/ml tetracycline. For crosslinking, cells were then exposed to UV light at 254 nm with an intensity of 2400 mJ/cm^2 or grown in media supplemented with 100 μM 4-thiouridine (Sigma-Aldrich) for 6 h prior to crosslinking at 365 nm in a Stratalinker with an intensity of 360 mJ/cm^2. The cells were lysed by sonication in IP buffer (50 mM Tris–HCl pH 7.4, 150 mM NaCl, 0.5 mM EDTA, 0.1% (v/v) Triton X-100 and 10% (v/v) glycerol) supplemented with 1X Roche cOmplete protease inhibitor. After centrifugation, the clarified lysate was added to anti-FLAG M2 magnetic beads that had been pre-equilibrated in IP buffer and samples were incubated for 2 h at 4°C. The beads were then washed five times with IP buffer then FLAG-tagged proteins and associated RNAs/proteins were eluted with 250 μg/ml of 3× FLAG peptide in 1× TBS for 1 h at 4°C. Eluates were ethanol-precipitated. Further sample processing was performed as described in (44) with minor modifications. Briefly, the protein-RNA pellet was dissolved in 4 M urea, 50 mM Tris–HCl pH 7.5 by sonication, following dilution to 1 M urea with 50 mM Tris–HCl pH 7.5. For RNA digestion, 500 U Pierce™ Universal Nuclease (Thermo Fisher Scientific) and 200 U nuclease p1 (NEB) were added following incubation at 37°C for 2 h. 10 μg RNase A (EN0531, Thermo Fisher Scientific) and 1U RNase T1 (Thermo Fisher Scientific) were added subsequently followed by 2 h incubation at 37°C. Proteins were digested overnight at 37°C using 4 μg trypsin (Promega). Sample cleanup was performed twice using C18 micro spin columns (Harvard Apparatus) according to the manufacturer's instructions. Briefly, samples were acidified to pH 3 using formic acid (FA) and adjusted to 2% (v/v) acetonitrile (ACN). After column equilibration, samples were loaded twice and washed three times with 5% (v/v) ACN, 0.1% (v/v) FA. Elution was performed in two steps using 80% (v/v) ACN, 0.1% (v/v) FA and 50% (v/v) ACN, 0.1% (v/v) FA. Eluates were dried in a speed vac concentrator. Crosslinked peptides were enriched using TiO_2 columns (in-house; Titansphere 5 μm; GL Sciences), as described previously (44). Briefly, samples were dissolved in buffer A (5% (v/v) glycerol, 80% (v/v) ACN, 5% (v/v) trifluoroacetic acid (TFA)) and loaded onto each three equilibrated TiO_2 columns. Washing was performed

three times with buffer A, three times with buffer B (60% (v/v) ACN, 5% (v/v) TFA) and once with 60% (v/v) ACN, 0.1% (v/v) TFA. Samples were eluted using ammonia solution and dried in a speed vac concentrator before LC-ESI–MS/MS analysis.

LC-ESI–MS/MS and data analysis of protein-RNA crosslinks

Enriched peptide-(oligo)nucleotides were dissolved in 2% (v/v) ACN, 0.05% (v/v) TFA. LC–MS/MS analyses were performed on an Orbitrap Exploris 480 (Thermo Fisher Scientific) instrument coupled to a nanoflow liquid chromatography system (UltiMate™ 3000 RSLCnano, Thermo Fisher Scientific). Sample separation was performed over 58 min at a flow rate of 300 nl/min using 0.1% (v/v) FA (buffer A) and 80% (v/v) ACN, 0.08% (v/v) FA (buffer B) and a linear gradient from 10% to 45% buffer B in 44 min. Eluting peptide-(oligo)nucleotides were analysed in positive mode using a data-dependent top 20 acquisition method. Resolution was set to 120 000 (MS1) and 30 000 FWHM (MS2); scan range (m/z), 350–1600; AGC targets, 10^6 (MS1) and 10^5 (MS2); normalized collision energy, 28%; dynamic exclusion, 9 s; maximum injection time, 60 (MS1) and 120 ms (MS2). Measurements were performed in two replicate injections. MS data were analysed and manually validated using the OpenMS pipeline RNPxl and OpenMS TOPPASViewer (44). Crosslink sites are reported at 1% spectrum level FDR.

AHA click labeling assay

For AHA click labelling (45), 7×10^5 cells were seeded into individual wells of a 6 well plate and grown overnight. The media was exchanged for methionine-free DMEM for 1 h and then 100 μM L-azidohomoalanine (AHA; Sigma Aldrich) was added for 3 h. Cells were washed twice with cold PBS and lysed by sonication in a buffer containing 50 mM Tris–HCl pH 8.0 and 0.5% SDS. The lysate was clarified by centrifugation at 20 000 × g at 4°C for 20 min. The protein concentration of the soluble extracts was determined using the Pierce™ BCA Protein Assay kit (ThermoFischer) and 150 μg of total protein from each sample was transferred to a fresh tube. 100 μM Biotin-Alkyne (Sigma-Aldrich), 1 mM TCEP (Sigma-Aldrich), 100 μM THPTA (Sigma-Aldrich) and 1 mM $CuSO_4$ (Sigma-Aldrich) were added to the protein samples, and the mixture was incubated at room temperature for 1 h. Proteins were precipitated using 20% (v/v) trichloroacetic acid (TCA) and separated by SDS-PAGE (12%). The biotinylated proteins were analysed by western blotting using IRDye® 800CW Streptavidin and, for normalization, the blot was probed with an anti-GAPDH antibody (Supplementary Table S4). Protein quantification was performed using the Image Studio Lite software (version 5.2.5).

Cell counting by analytical flow cytometry

Cell counting by analytical flow cytometry was performed as described in Kleiber et al., (46). WT and GP4KO HEK293 cells were seeded at equal density in six-well plates. Cells were harvested every 24 h by trypsinisation for 96 h, transferred to flow cytometry tubes, washed with 1XPBS and counted. Data acquisition and gating were performed using FACS Diva software (version 6.1.1) and data were exported using FlowCore (version 2.6.0).

RiboMeth-seq (RMS)

RiboMeth-seq was essentially performed as previously reported (47–49). In brief, 5 μg total RNA was fragmented under denaturing conditions using an alkaline buffer (pH 9.9). Subsequently, the RNA was separated on a denaturing (8 M urea) polyacrylamide gel, fragments in the size of 20–40 nt were excised and ligated to adapters using a modified tRNA ligase. cDNA was generated using Superscript III reverse transcriptase and sequenced on a PI Chip v3 using the Ion Proton platform. Reads were mapped to the human rDNA, snRNA, tRNA and snoRNA sequences, and the RMS score (fraction methylated) was calculated as 'score C' in (50), expect for cap-proximal methylations in snRNAs that was calculated according to (51). In a few cases, a barcode correction was applied when calculating the RMS score as described previously. The number of sequencing reads mapping to specific RNAs was used as a measure of their levels and is presented as reads per kilobase of transcript, per million mapped reads (RPKM) ± SEM. Statistical significance was determined using Student's t-test ($P < 0.05$).

RNase H-based cleavage assay to monitor 2′-*O*-methylation

The RNase H-based cleavage assay was performed as previously (24,52) with minor modifications. 250 ng of total RNA was denatured at 85°C for 3 min along with 1 pmol of chimeric 2′-*O* ribose methylated RNA-DNA oligonucleotide (Supplementary Table S6) in1X RNase H buffer (NEB) buffer. Samples were incubated on ice for 5 min, then mixed with 5 U of RNase H and incubated at 37°C for 30 min. Reactions were stopped by addition of 300 mM NaOAc pH 5.2 and 1 mM EDTA, and RNAs were extracted using PCI (25:24:1). The cleavage reaction products were resolved by denaturing agarose gel electrophoresis for monitoring sites on the 18S and 28S rRNAs or denaturing polyacrylamide gel electrophoresis in case of analysing sites on snRNAs. Cleavage products were detected by northern blotting using [^{32}P]-labelled DNA oligonucleotides probes as described above.

Results

The G-patch protein GPATCH4 is a stimulatory cofactor of the RNA helicase DHX15

Human cells express over 20 different G-patch proteins and several members of the protein family have been reported to bind DEAH box helicases via their G-patch domains (33). GPATCH4 contains an N-terminal G-patch domain and central coiled-coil (CC) domain (Figure 1A, left panel), but its cellular function and whether it functions as an RNA helicase cofactor remained unknown. It was recently reported that only a subset of RNA helicases, DHX15 (Figure 1A, right panel), DHX16 and DHX35, possesses the necessary amino acids to interact with G-patch proteins (35).

To investigate which of these DEAH box helicases GPATCH4 interacts with and to dissect which regions of GPATCH4 contribute to the interaction, stably transfected HEK293 Flp-In cell lines were generated for the inducible expression of C-terminally His-FLAG tagged wild-type GPATCH4 (GP4-His-FLAG) or derivatives. GPATCH4

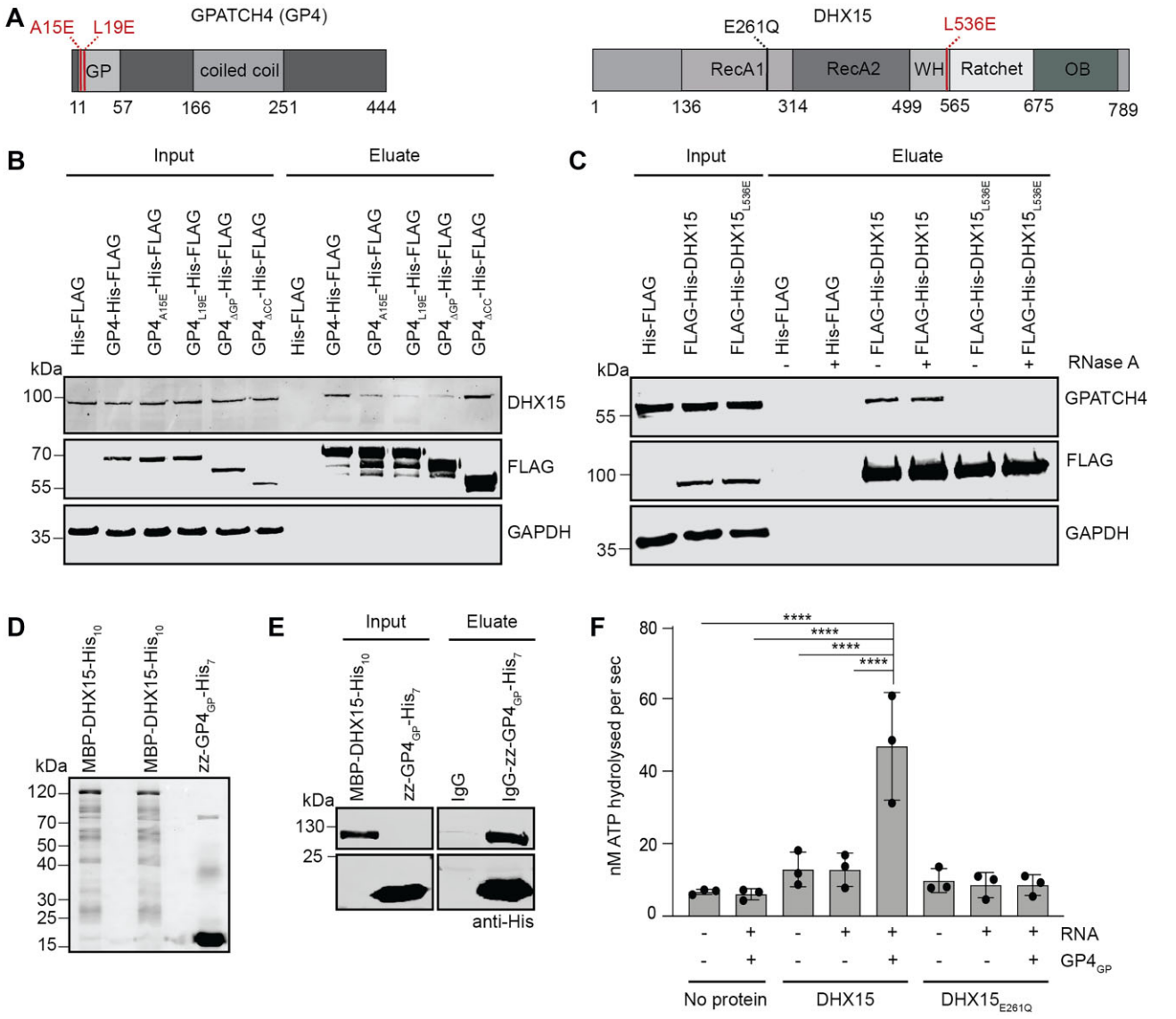

Figure 1. GPATCH4 binds the RNA helicase DHX15 and stimulates its ATPase activity. (**A**) Schematic views of the domain architectures of GPATCH4 (GP4) and DHX15. Domain boundaries according to UniProt (https://www.uniprot.org/) are indicated with amino acid numbers given below. Amino acid substitutions predicted to impede the interaction between GPATCH4 and DHX15 are indicated in red. An amino acid substitution within motif II of the DHX15 RecA1 domain known to reduce ATPase activity is indicated in black. (**B**) Whole cell extracts from stably transfected cell lines expressing the His-FLAG tag, or His-FLAG-tagged GPATCH4 or derivates thereof were used for anti-FLAG immunoprecipitations. Input (1%) and eluate samples were analysed by western blotting using the indicated antibodies. Experiments were performed in triplicate and representative data are shown. (**C**) Whole cell extracts from stably transfected cell lines expressing the His-FLAG tag or FLAG-His-tagged DHX15 or a derivate carrying an L536E substitution were used for anti-FLAG immunoprecipitations. Input (1%) and eluate samples were analysed by western blotting using the indicated antibodies. Experiments were performed in triplicate and representative data are shown. (**D**) Recombinant MBP-DHX15-His, MBP-DHX15$_{E261Q}$-His and ZZ-GP4$_{GP}$-His purified from *E. coli* were separated by SDS-PAGE and visualized by Coomassie staining. (**E**) MBP-DHX15-His was incubated with ZZ-GP4$_{GP}$-His-bound IgG or unbound IgG. Input (10%) and eluates were separated by SDS-PAGE and proteins were visualized by western blotting with an anti-His antibody. Experiments were performed in triplicate and representative data are shown. (**F**) ATP hydrolysis by MBP-DHX15-His, MBP-DHX15$_{E261Q}$-His in the absence (-) and presence (+) of a model RNA substrate and/or ZZ-GP4$_{GP}$-His were monitored using an NADH-coupled ATPase assay. ATPase activity of ZZ-GP4$_{GP}$-His was also analysed. Data from three independent experiments are shown as mean ± standard deviation (error bars) and individual data points are indicated by dots. Statistical analyses were performed using one-way ANOVA ($F = 14.6$, p value < 0.0001) and significance was calculated using Tukey's multiple comparisons test. The significance for selected pairs of samples is indicated as follows: **** $p < 0.0001$. p values for all comparisons are shown in Supplementary Table S7.

versions lacking either the G-patch or CC domains ($GP4_{\Delta GP}$ and $GP4_{\Delta CC}$, respectively) were expressed as well as variants containing single amino acid substitutions in the G-patch domain that, based on structural modelling analyses (Supplementary Figure S1A) would be expected to perturb a helicase-G-patch interaction ($GP4_{A15E}$-His-FLAG and $GP4_{L19E}$-His-FLAG). First, extracts from the cell line expressing GP4-His-FLAG and a control cell line expressing only the His-FLAG tag, were used for anti-FLAG immunoprecipitation (IP) experiments. Western blot analyses of the eluates using antibodies against DHX15, DHX16 and DHX35 revealed that wild-type GP4-His-FLAG efficiently immunoprecipitated DHX15 (Supplementary Figure S1B). Focusing then on DHX15, further IP experiments were performed using extracts from the cell lines expressing the truncated versions of GPATCH4. Lack of the CC domain did not perturb the GPATCH4-DHX15 interaction (Figure 1B). However, the absence of the G-patch domain or expression of the G-patch variants $GP4_{A15E}$-His-FLAG or $GP4_{L19E}$-His-FLAG substantially decreased the amount of DHX15 recovered (Figure 1B), demonstrating that the G-patch domain of GPATCH4 strongly contributes to the interaction with DHX15.

Reciprocal IP experiments were performed using extracts from stably transfected cell lines expressing N-terminally FLAG-His-tagged wild-type DHX15 or a version carrying a single amino acid substitution in the winged helix (WH) domain that has been shown to interact with residues in the G-patch domain of NKRF (FLAG-His-$DHX15_{L536E}$) (35) (Figure 1A, right; Supplementary Figure S1A). As expected, immunoprecipitation of wild-type FLAG-His-DHX15 recovered GPATCH4 (Figure 1C). The L536E amino acid substitution in DHX15 abolished the interaction with GPATCH4 (Figure 1C), supporting that DHX15 interacts with GPATCH4 in a similar way to other G-patch proteins (Supplementary Figure S1A). Moreover, treatment with RNase A had no influence on the amount of GPATCH4 recovered with FLAG-His-DHX15, implying that the interaction between these proteins is not bridged by RNA (Figure 1C).

The co-enrichment of GPATCH4 and DHX15 from cellular extracts demonstrates that they are in common complexes, but to determine whether they interact directly and form a stable complex alone, *in vitro* binding assays were performed. Recombinant expression and purification of full-length GPATCH4 from *E. coli* proved challenging due to its highly disordered nature (Supplementary Figure S1C). However, purified MBP-DHX15-His_{10} and an N-terminally ZZ- and C-terminally His_7-tagged version of the G-patch domain of GPATCH4 ($GP4_{GP}$) were obtained (Figure 1D). ZZ-$GP4_{GP}$-His_7 was immobilised and incubated with MBP-DHX15-His_{10}. Both ZZ-$GP4_{GP}$-His_7 and MBP-DHX15-His_{10} were recovered upon elution (Figure 1E), indicating that $GP4_{GP}$ stably associates with the helicase *in vitro*.

Some G-patch proteins have been shown to exert stimulatory effects on the activity of their helicase partner (see for example, (27,53–55)). To investigate whether GPATCH4 is a regulatory cofactor of DHX15, the effect of the $GP4_{GP}$ on the ATPase activity of DHX15 was examined. *In vitro* ATPase assays were performed using purified MBP-DHX15-His_{10} and a previously characterized (27) catalytically inactive version MBP-$DHX15_{E261Q}$-His_{10}, which has a glutamic acid to glutamine substitution in the ATP binding and hydrolysis motif II. MBP-DHX15-His_{10} displayed minimal ATPase activity in the presence and absence of a model RNA substrate. However, addition of ZZ-$GP4_{GP}$-His_7, which alone does not hydrolyse ATP, stimulated the ATPase activity of MBP-DHX15-His_{10} more than 3-fold (Figure 1F; Supplementary Table S7). By contrast, the ATPase activity of MBP-$DHX15_{E261Q}$-His_{10} was lower than that of the wild-type protein both in the presence and absence of RNA, and addition of $GP4_{GP}$ had no effect (Figure 1F).

Collectively, these data demonstrate that GPATCH4 is a cofactor of DHX15 that interacts via its G-patch domain to stimulate its ATPase activity.

GPATCH4 and DHX15 interact in the nucleolus and co-migrate with pre-ribosomal particles

DHX15 is a multifunctional RNA helicase present in different cellular compartments. To gain insight into where the interaction between GPATCH4 and DHX15 takes place, immunofluorescence was performed on HEK293 cells using antibodies against endogenous GPATCH4 and DHX15. Consistent with earlier reports, DHX15 was detected throughout the nucleoplasm (Figure 2A) (27). By contrast, GPATCH4 was predominantly present in nucleoli (Figure 2A, upper panel). Both DHX15 and GPATCH4 have been reported to be present in Cajal bodies (37,55,56). While some co-localisation of DHX15 with Cajal bodies was observed (Figure 2A, lower panel), the presence of endogenous GPATCH4 in Cajal bodies could not be detected. This is likely because it is present at levels below the detection limit of the experiment.

The presence of both GPATCH4 and DHX15 in nucleoli strongly suggests that this is a site of interaction. Therefore, to verify whether the two proteins form a complex in the nucleolus, IP experiments were performed using a nucleolar extract. Sub-cellular fractionation of HEK293 cell lines expressing His-FLAG or GP4-His-FLAG was performed; the purity of different fractions was verified using antibodies against marker proteins for key compartments, and both endogenous and His-FLAG-tagged GPATCH4 were confirmed to be enriched in nucleoli (Figure 2B). DHX15 was specifically recovered in the eluate of the anti-FLAG IP performed using the nucleolar extract from the cells expressing GP4-His-FLAG (Figure 2C), thereby confirming that GPATCH4 and DHX15 interact in the nucleolus.

As the nucleolus is the main site of ribosome assembly, a process in which DHX15 is implicated (27,57), we explored whether GPATCH4 associates with pre-ribosomal particles. Sucrose density gradient centrifugation was used to separate (pre-)ribosomal particles within HEK293 cell extracts from non-ribosome-associated material. The absorbance of the fractions was measured to identify the fractions containing (pre-)40S, (pre-)60S and 80/90S particles, which were confirmed by western blotting using antibodies against RPs and assembly factors present in different particles as well as northern blotting to detect mature and precursor rRNAs (Figure 2D; Supplementary Figure S2A). Western blotting using DHX15 and GPATCH4 antibodies revealed that both proteins co-migrate with pre-ribosomal subunits (Figure 2D). DHX15 was present in fractions containing

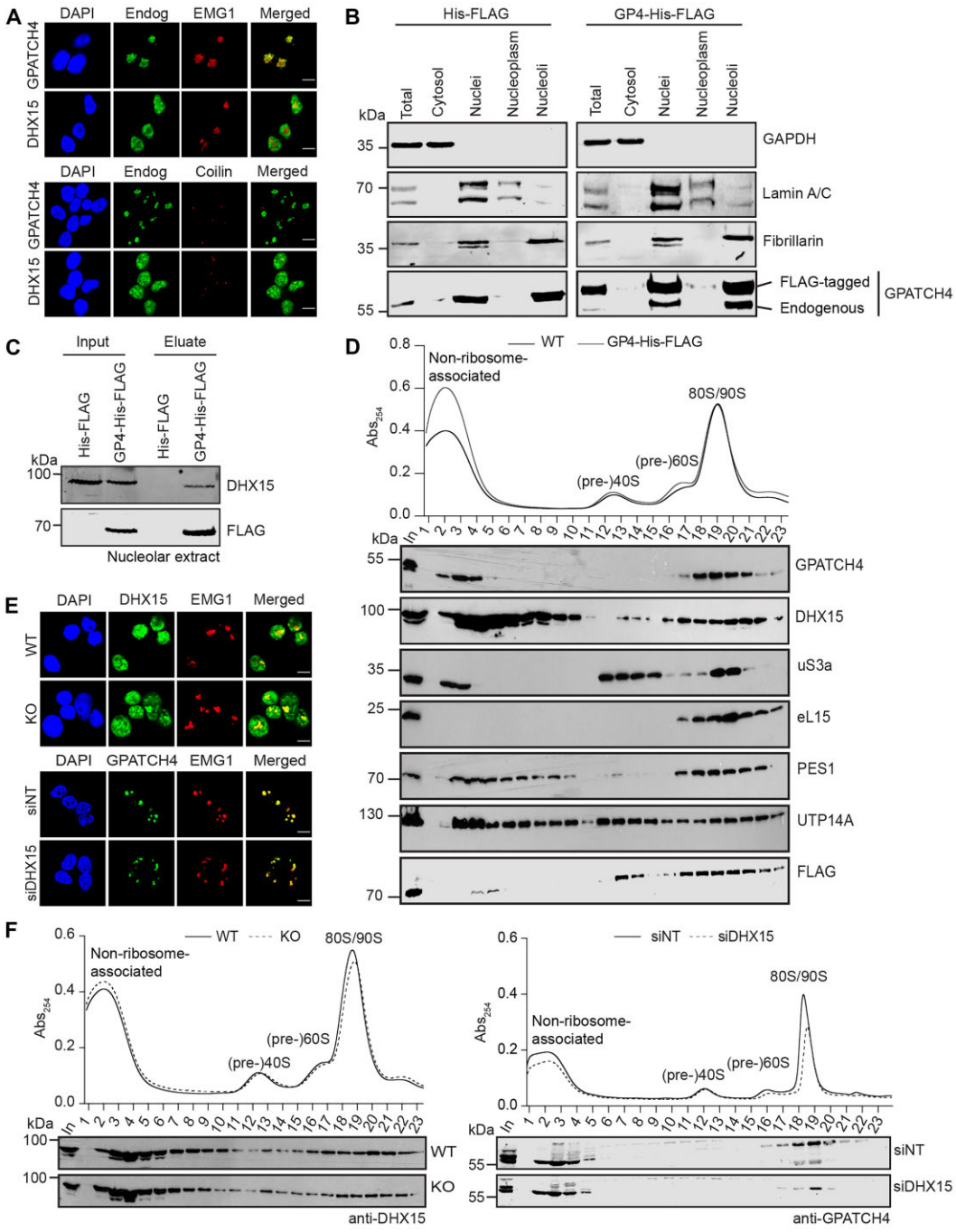

Figure 2. GPATCH4 and DHX15 interact in the nucleolus and co-migrate with pre-ribosomal particles. (**A**) HEK293 Flp-In cells (WT) were subjected to immunofluorescence using anti-GPATCH4 and anti-DHX15 antibodies. Nucleoli and Cajal bodies were identified using antibodies against EMG1 and coilin, respectively. Nuclear material was visualized using DAPI staining. Scale bar indicates 10 μm. Experiments were performed in triplicate and representative data are shown. (**B**) A nucleolar extract was prepared from WT cells expressing either the His-FLAG tag or GP4-His-FLAG. A cleared cell lysate (Total) was fractionated into cytosol and nuclei. Nuclei were then further fractionated into nucleoplasm and nucleoli. Samples taken throughout the fractionation procedure were analysed by western blotting using antibodies against GPATCH4 and characterized marker proteins for each cellular compartment (GAPDH - cytosol, Lamin A/C - nucleoplasm and fibrillarin – nucleoli). Experiments were performed in triplicate and representative data are shown. (**C**) Nucleolar extracts from the HEK293 cell lines expressing the His-FLAG tag or GP4-His-FLAG were used for anti-FLAG immunoprecipitation experiments. Input (1%) and eluates were analysed by western blotting using the indicated antibodies. Experiments were performed in triplicate and representative data are shown. (**D**) Total cell extracts from WT and those expressing GP4-His-FLAG were separated by sucrose density gradient centrifugation. Peaks corresponding to (pre-)ribosomal complexes are marked on an absorbance profile at 254 nm (top). Proteins present in the cell extract (In) and each fraction were subjected to western blotting using the indicated antibodies at the bottom. Marker proteins for different complexes: uS3a - (pre-)40S, UTP14A - pre-40S/90S (46), eL15 - (pre-)60S, and PES1 - pre-60S (47). Experiments were performed in triplicate and representative data are shown. The profile and blots for marker proteins are shown for the WT sample. (**E**) WT cells or those lacking GPATCH4 (GP4KO) as well as HEK293 cells treated with non-target siRNAs (siNT) or those targeting DHX15 (siDHX15) were subjected to immunofluorescence using antibodies against GPATCH4 and DHX15. Nucleoli were identified using antibodies against EMG1. Nuclear material was visualized using DAPI staining. Scale bar indicates 10 μm. Experiments were performed in triplicate and representative data are shown. (**F**) Total cell extracts from cells as in (**E**) were separated be sucrose density gradient centrifugation and analysed as in (D). Experiments were performed in duplicate and representative data are shown.

non-ribosomal complexes, likely reflecting free protein and spliceosomal complexes, as well as those containing pre-40S, pre-60S and 90S particles. GPATCH4 was predominantly found in fractions containing 90S particles. Importantly, the migration pattern of GP4-His-FLAG was similar to that of the endogenous protein, demonstrating that the presence of His-FLAG tag does not affect its association with pre-ribosomal particles (Figure 2D). These data suggest that the GPATCH4-DHX15 complex likely functions in the nucleolus during the early stages of ribosomal subunit assembly.

Some RNA helicase cofactors play roles in recruiting RNA helicases to appropriate substrate RNAs (e.g. (58)). The requirement of GPATCH4 and DHX15 for recruitment of each other to the nucleolus and pre-ribosomal particles were therefore explored. For this, a HEK293 cell line lacking GPATCH4 was generated using CRISPR/Cas9 genome editing (Supplementary Figure S2B; (38)). The GP4KO cell line contains a one basepair (bp) insertion followed by a one basepair substitution in exon 3 of *GPATCH4*, which leads to a translational frameshift and a premature stop codon (p.Thr38Isofs*16; Supplementary Figure S2C). Generation of a DHX15 knockout cell line was not possible, suggesting this protein is likely essential. Therefore, an RNAi-mediated depletion approach was used to deplete DHX15 to less than 10% of its normal level (Supplementary Figure S2D). Interestingly, while GP4KO did not alter the level of DHX15 (Supplementary Figure S2B), knockdown of DHX15 reduced the GPATCH4 protein level by 40% (Supplementary Figure S2D). As DHX15 functions in pre-mRNA splicing, it remains unclear whether this is an indirect effect or whether it reflects an interdependency of GPATCH4 and DHX15 on the protein level. The effect of lack of DHX15 or GPATCH4 on the subcellular localisation and pre-ribosome association of the other was then analysed using immunofluorescence and sucrose density gradient centrifugation followed by western blotting, respectively. The nucleolar localisation of both GPATCH4 and DHX15 remained unaffected when the other was depleted (Figure 2E). GP4KO also had no appreciable effect on DHX15 migration within sucrose gradients (Figure 2F). However, depletion of DHX15 lead to reduced co-migration of GPATCH4 with pre-ribosomal particles, indicated by a redistribution of the protein from later fractions to those containing non-ribosome-associated proteins (Figure 2F; Supplementary Figure S2E).

Taken together, these results reveal that GPATCH4 and DHX15 interact in the nucleolus and co-migrate with pre-ribosomal complexes, wherein lack of DHX15 reduces pre-ribosome association of GPATCH4.

GPATCH4 associates with rDNA and nascent pre-rRNA

The association of GPATCH4 with 90S pre-ribosomal particles (Figure 2D) implies a function during early ribosome assembly and/or rDNA transcription. The conditions used for the sucrose gradient analysis of pre-ribosome association only allow proteins associated with soluble particles to be detected. Therefore, to explore whether GPATCH4 associates with rDNA to coordinate co-transcriptional ribosome maturation events, we employed chromatin immunoprecipitation followed by high-throughput DNA sequencing (ChIP-seq). Experiments were performed using the GP4-His-FLAG cell line and, as a positive control, a cell line expressing NOLC1-His-FLAG (also known as NOPP140), a nucleolar chaperone that has been previously reported to bind rDNA (59). After protein-DNA and protein-protein crosslinking, chromatin shearing was performed and DNA-protein complexes were isolated. DNA was extracted, treated with Proteinase K and ligated to adapters for next-generation sequencing (NGS). The obtained sequencing reads were mapped to the human rDNA sequence. Compared to the His-FLAG negative control, the NOLC1-His-FLAG and, to an even greater extent, the GP4-His-FLAG samples contained an increased number of reads mapping to the transcribed rDNA locus (Figure 3A). For most of the intergenic sequence (IGS), no significant enrichment of mapped reads was observed, however, in the GP4-His-FLAG sample, a peak was detected towards the 3′ end of the IGS that partially overlaps with the rDNA promoter of the downstream rDNA repeat (Figure 3A). This suggests that GPATCH4 may associate with the rDNA promoter as the nascent pre-rRNA is being transcribed.

The finding that GP4-His-FLAG associates with the transcribed region of the rDNA locus, prompted us to investigate interactions of GPATCH4 with RNAs. The UV crosslinking and analysis of cDNA (CRAC) approach has been used to identify the pre-ribosomal binding sites of various ribosome assembly factors (27,60–62) so it was applied for GPATCH4. Crosslinked protein-RNA complexes were immunoprecipitated from HEK293 cell lines expressing GP4-His-FLAG or, as a control, the His-FLAG tag. Partial RNase digestion yielded crosslinked RNA fragments protected by protein binding, which were 5′ labelled with [^{32}P]. Following separation of enriched protein-RNA complexes by denaturing polyacrylamide gel electrophoresis (PAGE), radioactively labelled RNA fragments migrating at and above the anticipated size were detected only in the GP4-His-FLAG sample (Figure 3B). Appropriate areas of the membrane were excised, and RNA fragments were extracted and reverse transcribed to produce a cDNA library that was subject to NGS. After quality control and batch effect normalization, the obtained sequencing reads were mapped to human genome to enable identification of the crosslinked RNAs. Mapped reads in GP4-His-FLAG sample were normalised to those of the His-FLAG control and significant peaks with an adjusted p-value < 0.05 and $\log_2$ fold change > 2 were selected (Supplementary Table S8). Analysis of peak distribution across different classes of RNAs revealed that the majority of reads were derived from rRNAs and snoRNAs (Figure 3C; Supplementary Table S9). Inspection of the GP4-His-FLAG peaks on the pre-rRNA transcript revealed various crosslinking sites in the 28S rRNA as well as in the 5′ ETS and ITS2, which are present in pre-rRNA transcripts but then removed during pre-rRNA processing (Figure 3D). This is in line with the recently reported findings using the Targeted RNase H-mediated Extraction of crosslinked(X) RBPs' (TREX) approach, in which GPATCH4 was found crosslinked to various different regions of the pre-rRNA (63).

Collectively, these data suggest that GPATCH4 associates with the transcribed rDNA locus and binds the nascent pre-RNA, implying a role in co-transcriptional ribosome maturation events.

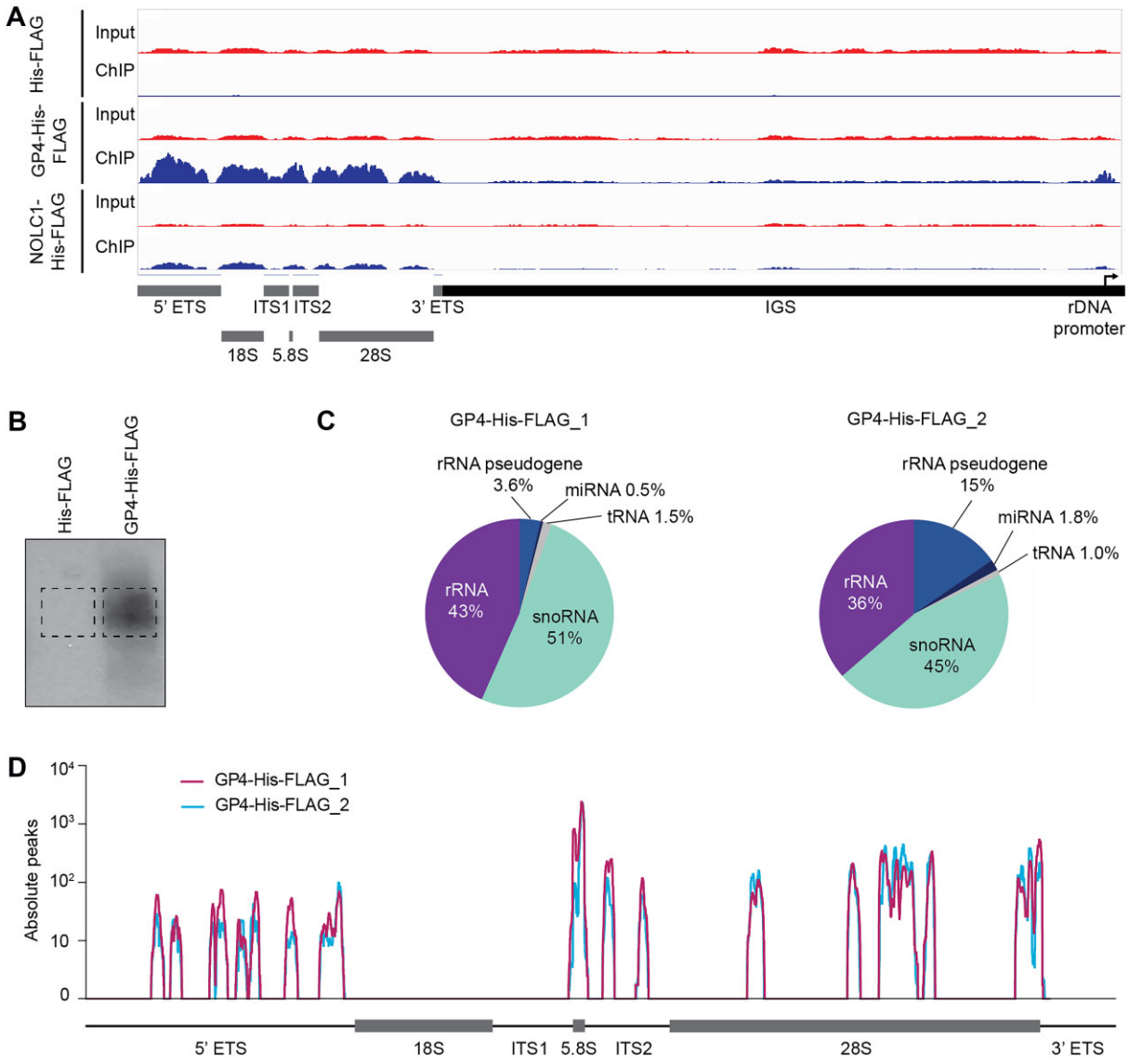

Figure 3. GPATCH4 associates with rDNA and pre-rRNA. (**A**) HEK293 cell lines expressing the His-FLAG tag, GP4-HisFLAG or, as a positive control NOLC1-His-FLAG, were crosslinked using EGS and PFA and subjected to chromatin immunoprecipitation (ChIP) via the FLAG tag. Sequencing reads were mapped to the rDNA locus and coverage tracks (scale for all tracks, 0–20 RPM) are shown above a schematic view of the rDNA locus. Two independent experiments were performed and data from one replicate (paired-end sequencing) are shown. (**B**) HEK293 cell lines expressing the His-FLAG tag or GP4-His-FLAG were UV crosslinked and RNA-protein complexes were enriched by anti-FLAG immunoprecipitation. Co-purified RNAs were trimmed, 5′ end labelled with [^{32}P] and ligated to sequencing adaptors. Complexes were separated by denaturing PAGE, transferred to nitrocellulose membrane and labelled RNAs were detected by autoradiography. Boxes indicate the areas of the membrane excised for further analysis. Two independent experiments were performed and representative data are shown. (**C**) Sequencing reads were mapped to the human genome and significant peaks present in the GP4-His-FLAG_1 and GP4-His-FLAG_2 samples that did not overlap with significant peaks in the FLAG sample were used for further analyses. Shown are the relative numbers of reads derived from different types of RNA. Abbreviations: miRNA – microRNA; rRNA – (pre-)ribosomal RNA; snoRNA – small nucleolar RNA; tRNA – transfer RNA. (**D**) Peaks on the rDNA region encoding the 47S pre-rRNA that are significant in the two GP4-His-FLAG datasets compared to the two His-FLAG datasets are shown above a schematic view of the pre-rRNA transcript. Mature rRNA sequences are shown as rectangle, and external transcribed spacers (5′ ETS and 3′ ETS) and internal transcribed spacers (ITS1 and ITS2) are depicted as black lines.

Components of the snoRNP machinery are associated with GPATCH4

In addition to reads derived from pre-rRNAs, a substantial proportion of CRAC reads in significant peaks derived from snoRNAs (Supplementary Tables S9 and S10). The indication that GPATCH4 associates with snoRNAs prompted us to explore the small RNA interactome of GPATCH4 using a focused RNA-IP (RIP) approach combined with deep sequencing. Anti-FLAG IPs were performed using extracts from HEK293 cell lines expressing GP4-His-FLAG or the His-FLAG control. Total RNA from the IP eluates were enriched for RNAs <200 nt in length, which were then subjected to small RNA-seq. Following quality control and normalisation, transcripts enriched with an adjusted P-value < 0.05 in the GP4-His-FLAG eluate compared to the control sample were identified. When comparing the types of small RNA recovered, strikingly, 98.7% of the reads in significant peaks derived from snoRNAs and a small fraction (1.2%) mapped

to scaRNA genes (Figure 4A; Supplementary Table S11). Deeper analysis of the sub-type distribution of enriched snoRNAs revealed 248 candidates where 95% of the reads came from box C/D snoRNAs and 3% from snoRNAs of the H/ACA subfamily (Figure 4B; Supplementary Table S11). Importantly, all snoRNAs recovered in the CRAC experiment were also enriched with GP4-His-FLAG in the small RNA RIP-seq experiment (Supplementary Tables S10 and S12). To validate the association of GP4-His-FLAG with snoRNAs, RIP followed by northern blotting was performed for selected RNA targets observed to be enriched in the RIP-seq data (Supplementary Table S12), and $tRNA^{Met(CAU)}$ as a negative control. Notably, snoRNAs from both the box C/D and H/ACA subfamilies, as well as scaRNAs, were recovered with GPATCH4 (Figure 4C). As GPATCH4 has no canonical RNA-binding domain, how it interacts with RNA was investigated. Cells expressing GP4-His-FLAG were crosslinked using UV light at 254 nm or grown in the presence of 4-thiouridine then crosslinked with light at 365 nm, to stabilise RNA-protein interactions and complexes were recovered by anti-FLAG immunoprecipitation. The eluates were treated with RNase, digested with trypsin and subjected to mass spectrometry for identification of amino acid residues crosslinking to RNA. This highlighted two cysteine residues (C152 and C333) and one histidine (H385) that were crosslinked to nucleotides (Supplementary Table S13). Notably, these residues lie within the disordered regions of the protein (Figure 4D), which is in line with the notion that intrinsically disordered regions (IDRs) confer conformational flexibility to proteins, enabling them to serve as hubs for RNP formation (64).

As snoRNAs associate with various proteins to form functional snoRNP complexes, we explored whether GPATCH4 also associates with the catalytic components of box C/D and H/ACA snoRNPs (fibrillarin and dyskerin, respectively) as well as NOLC1 that is reported to function as a sno/scaRNP chaperone (65,66). Anti-FLAG IPs using extracts from cells expressing GP4-His-FLAG or the His-FLAG tag alone were conducted in the presence or absence of RNase A. Fibrillarin, dyskerin and NOLC1 were all specifically recovered with GP4-His-FLAG (Figure 4E). Notably, NOLC1 was recovered with GP4-His-FLAG much more efficiently than either fibrillarin or dsykerin. RNase A treatment disrupted the interactions of GPATCH4 with fibrillarin and dyskerin, suggesting that they are bridged by RNA (Figure 4E). By contrast, the association of GP4-His-FLAG with NOLC1 was not affected, implying that this interaction is mediated via protein-protein contacts (Figure 4E). Taken together, these results reveal that GPATCH4 is an RNA-binding protein that interacts with snoRNPs, potentially during synthesis of the pre-rRNA transcript.

GPATCH4 is required for efficient 2′-*O*-methylation of specific rRNA and snRNA residues and protein synthesis

The findings that GPATCH4 co-migrates with pre-ribosomal subunits in sucrose gradients, and directly associates with the transcribed rDNA, pre-rRNAs and snoRNPs implies that it functions during the early stages of ribosome assembly. Perturbed ribosome biogenesis can manifest as defects in rRNA maturation so the effect of loss of GPATCH4 on the steady-state levels of pre-rRNA intermediates (Supplementary Figure S3A) and nascent (pre-)rRNA synthesis were monitored by northern blotting and pulse chase metabolic labelling. Lack of GPATCH4 did not affect either pre-rRNA processing or the production of the mature 18S and 28S rRNAs (Figure 5A; Supplementary Figures S3B).

To determine if ribosome function is nevertheless affected by lack of GPATCH4, nascent protein synthesis was monitored by determining the incorporation of azidohomoalanine (AHA), a methionine analogue, which can be detected by biotin labelling via a click chemistry approach. Compare to wild-type HEK293 cells, GP4KO cells displayed significantly reduced protein synthesis (Figure 5B), suggesting that ribosome function is impaired by the absence of GPATCH4. As assembly of ribosomal subunits and protein synthesis are critical and highly energy-consuming processes (67), the effect of loss of GPATCH4 on cellular proliferation was investigated. Compared to wild-type HEK293 cells, GP4KO cells showed significantly reduced growth (Figure 5C; Supplementary Table S14), consistent with a role of GPATCH4 in the production of functional ribosomal subunits.

The association of GPATCH4 with modification-guide snoRNAs (Figure 4A–C; Supplementary Tables S10 and S12) raised the possibility that GPATCH4 infuences rRNA modification. As the majority of snoRNAs bound by GPATCH4 belonged to the box C/D subfamily, RiboMeth-seq (RMS) (47,50) was utilised to monitor 2′-*O*-methylation levels in abundant RNAs in both wild-type and GP4KO cells. Total RNA from wild-type and GP4KO cells was subjected to partial alkaline hydrolysis, and cleaved fragments were converted to a cDNA library that was deep sequenced. Based on mapping read ends, an RMS score for each 2′-*O*-methylated site was calculated. Strikingly, loss of GPATCH4 decreased modification at several sites on rRNAs and snRNAs (Figure 5D–G; Supplementary Table S15). Importantly, the snoRNAs/scaRNAs guiding modifications of the affected modification were all enriched in the GPATCH4 RIP (Figure 4C; Supplementary Table S12). The RIP data indicated that GPATCH4 also associates with H/ACA box snoRNAs, so we addressed whether GPATCH4 also regulates rRNA pseudouridylation. SNORA40 and SNORA81, which were strongly enriched with GPATCH4 (Figure 4C and Supplementary Table S12), guide formation of Ψ1174 in the 18S rRNA and Ψ4606 in the 28S rRNA, respectively. The extent of pseudouridylation of these sites in wild-type and GP4KO cells was therefore monitored using CMC-labelling of total RNA, followed by primer extension that produces cDNA fragments stopping 1 nucleotide before the CMC-Ψ adduct. Pseudouridylation of these sites was not affected by the absence of GPATCH4 (Supplementary Figure S4A, B). We cannot exclude a role for GPATCH4 in regulating other rRNA pseudouridylation events, however, these data suggest that GPATCH4 is likely dispensable for rRNA pseudouridylation but required for efficient formation of numerous rRNA and snRNA 2′-*O*-methylations.

To understand more about the 2′-*O*-methylations affected by lack of GPATCH4, their positions in the rRNAs were mapped onto the tertiary structure of the 80S ribosome (Supplementary Figure S5A). In line with the distribution of affected sites along the length of the rRNAs, this did not reveal any clear clustering. As GPATCH4 physically associates with snoRNPs (Figure 4A–C, D), a possible explanation for the observed reduction in 2′-*O*-methylation could be that the snoRNAs guiding these modifications are destabilised

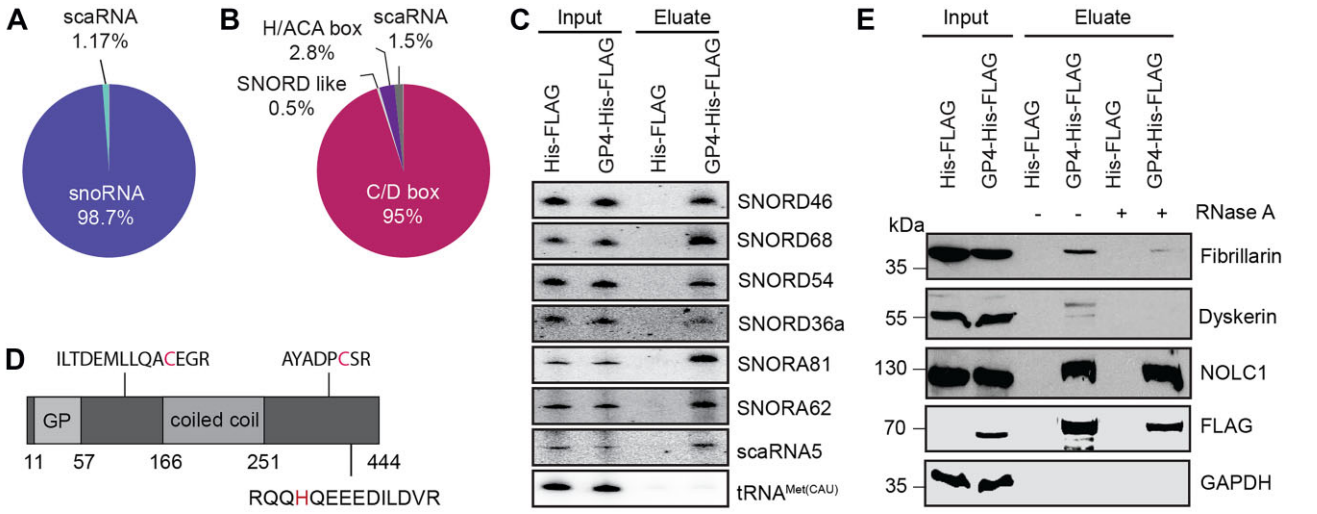

Figure 4. Components of the snoRNP machinery are bound by GPATCH4. (**A**) Extracts from HEK293 cells expressing the His-FLAG tag or GP4-His-FLAG were used for anti-FLAG immunoprecipitation experiments. RNAs extracted from the eluates were subjected to small RNA-seq. Two independent experiments were performed and averaged data are shown. The relative proportion of sequencing reads mapping to different types of small RNAs is shown. Abbreviations: snoRNA – small nucleolar RNA; scaRNA – small Cajal body-associated RNA. (**B**) The distribution of sequencing reads derived from different types of snoRNAs in the samples described in (A) is shown. (**C**) HEK293 cells expressing the His-FLAG tag or GP4-His-FLAG were UV crosslinked and whole cell extracts were used for anti-FLAG immunoprecipitation. RNAs present in inputs (0.5%) and eluates were separated by denaturing polyacrylamide gel electrophoresis and analysed by northern blotting to detect the indicated snoRNAs/scaRNAs, and $tRNA^{Met(CAU)}$ served as a negative control. Experiments were performed in triplicate and representative data are shown. (**D**) HEK293 cell expressing the His-FLAG tag or GP4-His-FLAG were UV crosslinked (254 nm) or cells were grown in the presence of 4-thiouridine and then crosslinked using light at 365 nm. Cleared extracts were then used for anti-FLAG immunoprecipitation. Eluates were protease- and RNase-treated and protein-RNA crosslinked peptides were identified by mass spectrometry. Amino acids of GPATCH4 crosslinked to nucleotides are indicated on a scheme of GPATCH4 with the domain architecture marked as in Figure 1A. (**E**) Whole cell extracts from HEK293 cells expressing the His-FLAG tag or GP4-His-FLAG were used for anti-FLAG immunoprecipitation in the absence (–) and presence (+) of RNase A. Input (1%) and eluate samples were analysed by western blotting using antibodies against the snoRNP-associated proteins indicated. Experiments were performed in duplicate and representative data are shown.

in the absence of GPATCH4. SnoRNA levels in the wild-type and GP4KO cells were therefore determined using the RMS sequencing reads as a measure of transcript coverage reflecting RNA abundance. No significant alterations in snoRNA levels were detected (Figure 5H-I), implying that reduced snoRNA availability does not underlie the reduced rRNA 2′-*O*-methylation. Consistent with the analyses of pre-rRNA levels by northern blotting and pulse-chase metabolic labelling (Figure 5A and Supplementary Figure S3B), the numbers of RMS reads derived from the 18S and 28S rRNAs were similar in the wild-type and GP4KO cell lines (Supplementary Figure S3C).

GPATCH4 associates with and regulates DHX15, whose yeast homologue Prp43 is required for efficient rRNA and snRNA 2′-*O*-methylation (23,24). Therefore, the effect of depletion of DHX15 on RNA 2′-*O*-methylation was also examined by RMS. Lack of DHX15 also lead to reduced 2′-*O*-methylation at numerous sites on the rRNAs and snRNAs (Supplementary Figure S5B-E; Supplementary Table S15). Importantly, good concordance between these results and those published by Duchemin *et al*., 2021 were observed (37). Comparing the 2′-*O*-methylations influenced by loss of GPATCH4 and DHX15 revealed sites that were affected by lack of both proteins as well as sites that were only affected by lack of one or the other protein. In conclusion, these data show that GPATCH4 functions in ensuring efficient 2′-*O*-methylation of rRNAs and snRNAs, but suggest that this role may only partially involve DHX15.

GPATCH4 regulates rRNA and snRNA 2′-*O*-methylation both dependent on, and independent of, its interaction with DHX15

The finding that both GPATCH4 and DHX15 are required for efficient 2′-*O*-methylation at some sites within the rRNAs and snRNAs raised the question of whether interaction between the two proteins is necessary in this context. To address this, a complementation system was established in which the GP4KO cell line was stably transfected with plasmids for the expression of GP4-His-FLAG or GPATCH4 defective in binding DHX15 ($GP4_{A15E}$-His-FLAG; Figure 1B). Both His-FLAG tagged proteins were expressed similarly to each other and at close to the same level as the endogenous protein (Supplementary Figure S6A). Using this system, the 2′-*O*-methylation status of specific sites was monitored using RNase H-based cleavage assays. In this approach, a chimeric RNA–DNA oligonucleotide is annealed to the target RNA region; treatment with RNase H leads to site-specific RNA cleavage of non-2′-*O*-methylated RNA-DNA hybrids but the presence of a 2′-*O*-methylated nucleotide in the target RNA prevents RNase H-mediated cleavage (52). Using this technique, the 2′-*O*-methylation levels of specific sites identified by RMS to depend on both GPATCH4 and DHX15 (18S-Gm644 and 28S-Cm2791) or GPATCH4 only (18S-Am668, U5-Um41 and U2-Um47) were monitored. These sites were selected based on, i) the robust effects of lack of GPATCH4 and/or DHX15 in the RMS data and ii) their suitability for RNase H-based cleavage assays (i.e. the lack of adjacent or closely proximal 2′-*O*-methylations)

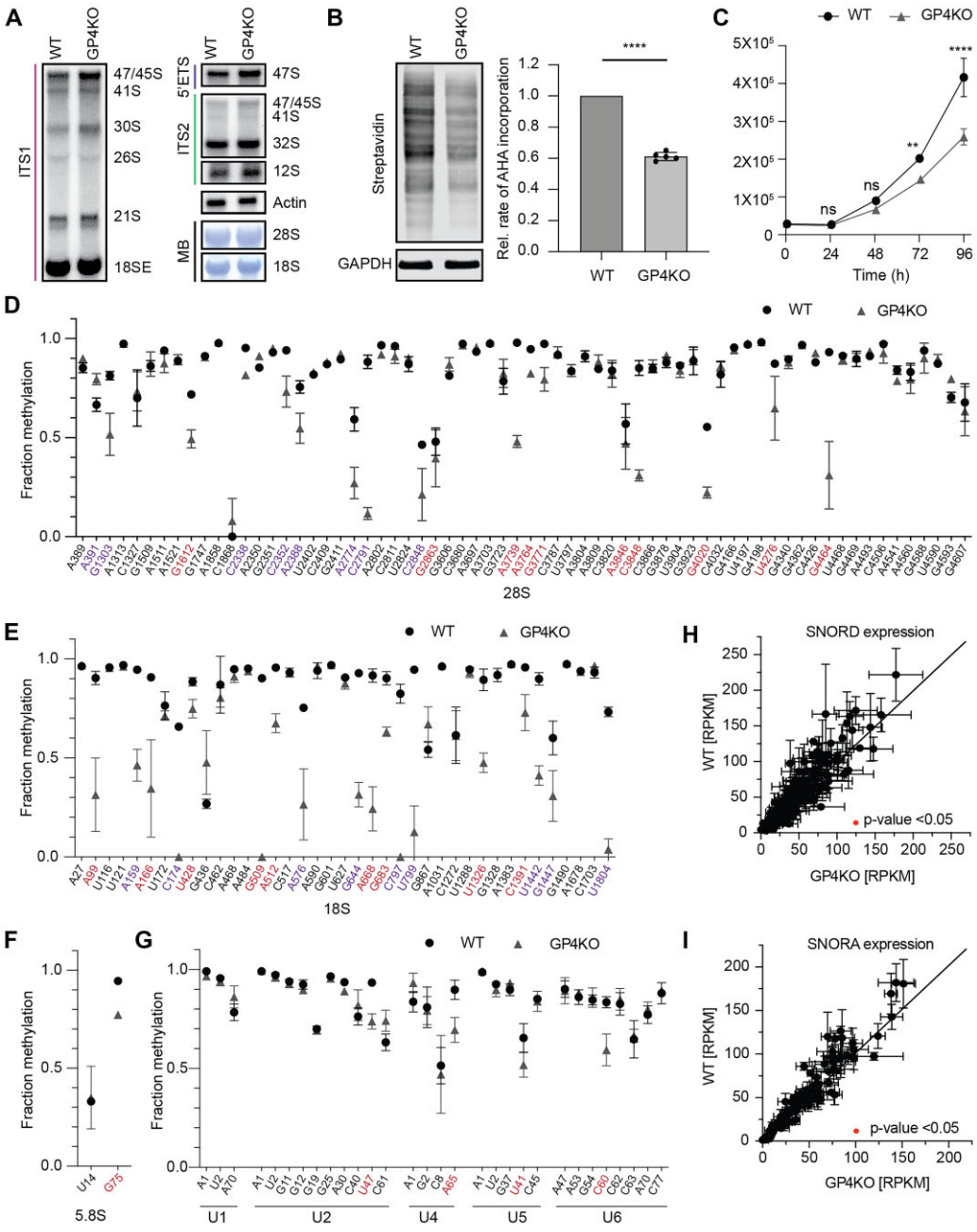

Figure 5. GPATCH4 is dispensable for pre-RNA processing but is required for efficient 2′-*O*-methylation of specific rRNA and snRNA residues. (**A**) Total RNA from wild-type HEK293 (WT) cells and those lacking GPATCH4 (GP4KO) was separated by denaturing agarose gel electrophoresis and major pre-rRNA intermediates were detected by northern blotting. The actin mRNA served as a loading control and mature rRNAs were visualized by methylene blue staining. Experiments were performed in triplicate and representative data are shown. (**B**) Wild-type HEK293 cells (WT) and those lacking GPATCH4 (GP4KO) were used for an AHA click labelling assay to monitor nascent protein synthesis. GAPDH levels were used for normalization. Five independent experiments were performed and representative data are shown. For quantification, data are presented as mean ± standard deviation. Statistical analyses were performed using a two-tailed unpaired Student t-test and significance between WT and GP4KO is indicated as follows: ****$p < 0.0001$. (**C**) The numbers of cells in equally seeded cultures of wild-type HEK293 cells (WT) and those lacking GPATCH4 (GP4KO) were determined at the indicated times after seeding. Three independent experiments were performed and data are shown as mean ± standard deviation. Statistical analyses were performed using two-way ANOVA and significance was calculated using Sidak's multiple comparison test. Significance between WT and GP4KO at a given time-point are indicated as follows: **$p < 0.001$, ****$p < 0.0001$ and n.s = non-significant. p values for all comparisons are given in Supplementary Table S14. (D–G) Total RNA from WT and GP4KO were subjected to RiboMeth-seq (RMS) analysis. Experiments were performed in triplicate and the mean RMS score, corresponding to the fraction methylated, is plotted for each 2′-*O*-methylated nucleotide in the 28S (**D**), 18S (**E**) and 5.8S (**F**) rRNAs and each snRNA of the major spliceosome (**G**). Note that 18S-U354, 18S-C1440 and 28S-A1310, which are 2′-*O*-methylated in differentiated cells but not or lowly methylated in cell lines (47,90), are not represented here as no methylation was detected. 28S-C1868 is included as it is usually methylated in cell lines, except for HEK293 cells (91). Error bars represent standard deviation. Sites affected by lack of GPATCH4 alone are marked in red and sites affected by lack of both GPATCH4 and DHX15 are marked in purple. (**H, I**) The number of sequencing reads mapping to each snoRNA (box C/D – H and box H/ACA – I) were determined in the RMS datasets for WT and GP4KO are expressed as reads per thousand mapped reads (RPKM). Relative snoRNA levels from three independent RMS experiments are shown as mean ± standard error of the mean.

For all tested sites, the RNase H-based cleavage assays confirmed the reduced 2′-*O*-methylation detected by RMS in the GP4KO cell line (Figure 5D, E, G and Figure 6A–E). Furthermore, re-expression of GP4-His-FLAG rescued these defects confirming that the reduced 2′-*O*-methylation arises due to lack of GPATCH4 (Figure 6A–E; Supplementary Table S16). In the case of 18S-Gm644 and 28S-Cm2791 that are affected by lack of both GPATCH4 and DHX15, expression of $GP4_{A15E}$-His-FLAG failed to rescue 2′-*O*-methylation, indicating that interaction between the two proteins is necessary (Figure 6A, B; Supplementary Table S16). By contrast, 2′-*O*-methylation of 18S-A668, U5-U41 and U2-U47, that were only affected by loss GPATCH4, was effectively restored by expression of the non-DHX15-interacting $GP4_{A15E}$-His-FLAG (Figure 6C–E; Supplementary Table S16).

As GPATCH4 stimulates the ATPase activity of DHX15 (Figure 1F), the finding that interaction between GPATCH4 and DHX15 is necessary for 2′-*O*-methylation of some rRNA nucleotides, raised the question of whether the catalytic activity of DHX15 contributes to efficient 2′-*O*-methylation at such sites. To investigate this, an RNAi-based complementation system was used in which endogenous DHX15 can be depleted and siRNA-insensitive, FLAG-His-tagged wild-type or catalytically inactive $DHX15_{E261Q}$ are expressed (Supplementary Figure S6B). Focusing on 18S-Gm644, consistent with the RMS data, we observed reduced 2′-*O*-methylation when DHX15 was depleted and restored modification upon re-expression of wild-type DHX15 (Figure 6F; Supplementary Table S16). However, expression of FLAG-His-$DHX15_{E261Q}$ failed to rescue methylation of 18S-G644, demonstrating that the catalytic activity of DHX15 contributes to regulating 2′-*O*-methylation at this site.

Taken together, these data show that GPATCH4 is important for rRNA and snRNA 2′-*O*-methylation in some cases independently, and in other cases dependent on its association with DHX15. The GPATCH4-stimulated catalytic activity of DHX15 is necessary for efficient methylation of some rRNA sites, defining a cellular function of this RNA helicase-cofactor complex.

Discussion

Regulation of RNA helicase activity is essential within the complex cellular environment to limit off-target effects and achieve target specificity. G-patch proteins have emerged as a family of RNA helicase cofactors that combine activation of specific cognate DEAH box helicases with their recruitment to appropriate substrate RNAs or RNPs (33). Here, we describe GPATCH4 as a G-patch protein cofactor of the multifunctional RNA helicase DHX15. Our data show that GPATCH4 associates with DHX15 using contacts common with other G-patch protein–RNA helicase complexes, suggesting that the observed stimulation of DHX15 ATPase activity by GPATCH4 occurs by the tethering the tandem RecA-like domains of DHX15 in an optimal conformation for ATP hydrolysis and translocation, as has been described for other G-patch protein cofactors (35,68). These G-patch protein contact sites are only present in three DEAH box helicases, DHX15, DHX16 and DHX35 (33,35), and intriguingly, the finding that GPATCH4 associates with and regulates DHX15 brings the number of identified G-patch protein cofactors of DHX15 to eleven (AGGF1, CMTR1, GPATCH2, NKRF, PINX1, RBM5, RBM17, SUGP1, TFIP11, ZGPAT, GPATCH4) (27,53–55,57,69–73). Based on the overlapping binding sites of these G-patch proteins, their interactions with the RNA helicase will be mutually exclusive and it is likely that the balance of cofactor expression levels determines the distribution of DHX15 between its different cellular functions, as has been proposed in yeast (74). Our data show that GPATCH4 and DHX15 localise to the nucleolus independently of each other. Lack of GPATCH4 does not strongly affect association of DHX15 with pre-ribosomal particles, but interestingly, the amount of GPATCH4 present on pre-ribosomes is reduced by depletion of DHX15. Beyond GPATCH4, DHX15 associates with other G-patch proteins in the context of ribosome assembly (NKRF, PINX1 and likely also GPATCH2; (27,57,70)). The minimal influence of GPATCH4 on DHX15 association with pre-ribosomes may therefore be explained by the contribution of several of these G-patch proteins to DHX15 pre-ribosome recruitment. This is supported by the previous observation of a mild reduction in DHX15 association with pre-ribosomes in cells depleted of NKRF (27). The finding that DHX15 influences recruitment of GPATCH4 to pre-ribosomes could suggest a direct role for the helicase in cofactor recruitment or it may be that another ribosome assembly event involving DHX15 is an essential pre-requisite for GPATCH4 association with pre-ribosomes.

Our data demonstrate a role for the GPATCH4-DHX15 complex in ensuring the efficient installation of a subset of snoRNA-guided rRNA 2′-*O*-methylations (Figure 7). Lack of GPATCH4 also influences the 2′-*O*-methylation of various other rRNA nucleotides and several sites within the U2, U4, U5 and U6 snRNAs, but these effects appear to be independent of its interaction with DHX15. There are several other examples of G-patch proteins that function both together with, and independently of, interactions with their cognate helicases. While NKRF and DHX15 are required for cleavage of the initial pre-rRNA transcript at site A', NKRF fulfils an additional role as a transcriptional repressor of NF-κB-regulated genes containing an NRE sequence in their promoters (27,75,76). Likewise, PINX1 and DHX15 function together in ribosome biogenesis (57), but PINX1 also acts as a telomerase inhibitor independently of its G-patch domain, and therefore its interaction with DHX15 (77). Likewise, TFIP11 acts together with DHX15 in the context of pre-mRNA splicing, but independently contributes to snRNA modification (37,72).

The finding that GPATCH4 is required for efficient 2′-*O*-methylation of both rRNAs and snRNAs mirrors the requirement of other factors, such as NOLC1 for modification of both types of RNA. In the context of snRNA modification, NOLC1 associates with scaRNAs to concentrate them in Cajal bodies (66,78), thereby promoting efficient snRNA 2′-*O*-methylation. NOLC1 is known to also physically associate with Pol I (79) where it has been proposed to function as a chaperone, ensuring functional snoRNP association with nascent transcripts. Notably, in stable knockdown HeLa cells (66), lack of NOLC1 was observed to impact the 2′-*O*-methylation of numerous snRNAs sites, but the effects on rRNA 2′-*O*-methylation were minimal and most of the rRNA 2′-*O*-methylations affected by lack of NOLC1 are naturally hypomethylated sites. In contrast to NOLC1, the effects GPATCH4 KO are more pronounced on rRNAs than snRNAs. Although the lack of overlap between the GPATCH4 and NOLC1 RMS datasets may reflect differences in the

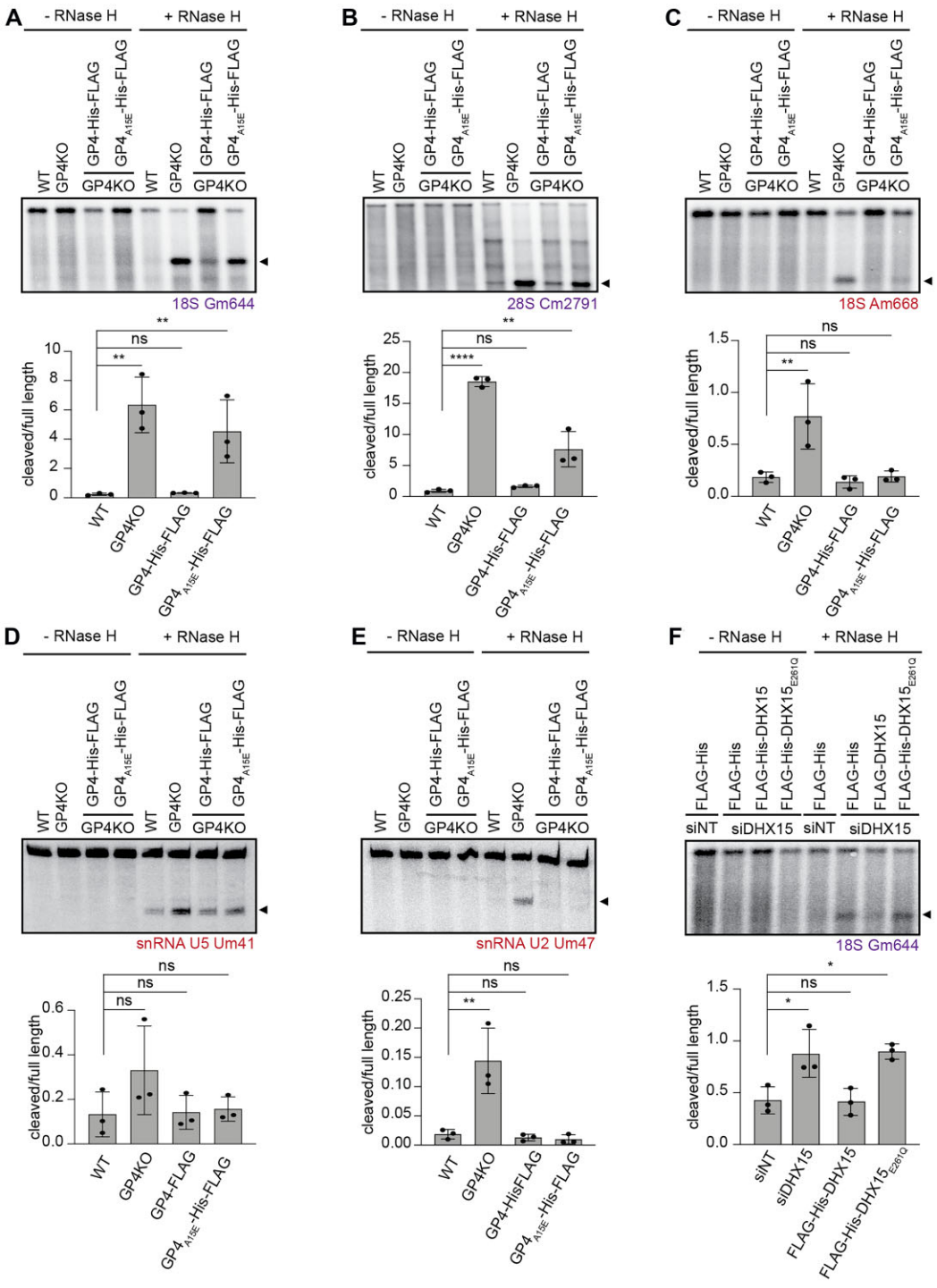

Figure 6. GPATCH4 regulates rRNA and snRNA 2′-*O*-methylation in DHX15-dependent and -independent manners. (A–E) Total RNA from wild-type HEK293 cells (WT), cells lacking GPATCH4 (GP4KO) and the GP4KO cell line complemented with expression of wild-type GP4-His-FLAG or the version of GPATCH4 that is impaired in DHX15 interaction ($GP4_{A15E}$-His-FLAG) was annealed to chimeric RNA-DNA oligonucleotides targeting RNase H cleavage of 18S Gm644 (**A**), 28S Cm2791 (**B**), 18S Am668 (**C**), U5 Um41 (**D**), U2 Um47 (**E**). Samples were left untreated (-) or were treated with RNase H (+). RNAs were separated by denaturing agarose (A–C) or acrylamide (D, E) gel electrophoresis, and cleaved and uncleaved RNAs were detected by northern blotting. Data from three independent experiments is shown as mean ± standard deviation (error bars) and individual data points are indicated by dots. Statistical analyses were performed using one-way ANOVA and significance is indicated as follows: $^{**}p < 0.01$, $^{****}p < 0.0001$, and ns = not significant. *p* values for all comparisons are shown in Supplementary Table S16. Sites affected by lack GPATCH4 alone are marked in red and sites affected by lack of both GPATCH4 and DHX15 are marked in purple. (**F**) HEK293 cells expressing the FLAG tag were treated with non-target siRNAs (siNT) or siRNAs targeting DHX15 (siDHX15) and stably transfected cell lines expressing FLAG-DHX15 or the catalytically inactive derivative ($FLAG\text{-}DHX15_{E261Q}$) at close to endogenous levels were treated with siDHX15. Total RNA was extracted and annealed to chimeric RNA-DNA oligonucleotides targeting RNase H cleavage of 18S Gm644. Samples were left untreated (–) or were treated with RNase H (+). RNAs were separated by denaturing agarose gel electrophoresis, and cleaved and uncleaved RNAs were detected by northern blotting. Data from three independent experiments is shown as mean ± standard deviation (error bars) and individual data points are indicated by dots. Statistical analyses were performed using one-way ANOVA and significance is indicated as follows: $^{*}p < 0.05$ and ns = not significant. *p* values for all comparisons are shown in Supplementary Table S16.

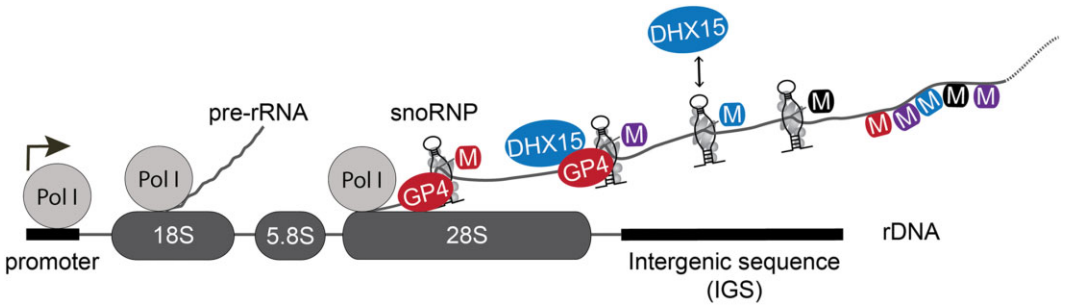

Figure 7. Schematic model of the DHX15-dependent and DHX15-independent roles of GPATCH4 in ensuring efficient rRNA 2′-*O*-methylation. RNA polymerase I (Pol I) binds the rDNA promoter (black rectangle) to synthesize nascent pre-rRNA. GPATCH4 (GP4) associates with the transcribed region of the rDNA, the pre-rRNA transcript and box C/D snoRNPs (indicated by a black hairpin RNA with associated proteins in grey). The extent of rRNA 2′-*O*-methylation is affected at some sites by loss of GPATCH4 (M in red box), lack of DHX15 (M in blue box) or disruption of interactions between GPATCH4 and DHX15 (M in purple box). Some rRNA 2′-*O*-methylations are unaffected by lack of either GPATCH4 or DHX15 (M in black box).

nature of protein depletion or the cell line backgrounds, the available data suggest that GPATCH4 and NOLC1 affect different subsets of modifications. Rather than directly functioning together to influence the installation of specific 2′-*O*-methylations, it is likely, therefore, that GPATCH4 and NOLC1 act analogously and/or complementarily. The robust immunoprecipitation of NOLC1 with GPATCH4 may reflect the association of both these proteins with the rDNA promoter and the nascent pre-rRNA transcript, where they are poised to chaperone specific snoRNA-guided 2′-*O*-methylations.

Interestingly, NOLC1 associates with both 2′-*O*-methylation-guiding box C/D and pseudouridylation-guiding box H/ACA sno/scaRNAs. While our data demonstrate that GPATCH4 predominantly associates with box C/D sno/scaRNAs, some box H/ACA sno/scaRNAs were also recovered in RIP-seq experiments and were confirmed to associate with GPATCH4 by northern blotting. GPATCH4 also displays RNA-dependent interactions with both fibrillarin and dyskerin in immunoprecipitations experiments, further supporting its association with both box C/D and box H/ACA snoRNPs. Despite the interaction of GPATCH4 with some H/ACA snoRNPs, analysis of rRNA pseudouridylations guided by these snoRNPs demonstrate that the levels of these modifications are not affected by lack GPATCH4. This is similar to the previous finding that although NOLC1 associates with both box C/D and box H/ACA scaRNAs, lack of NOLC1 affects snRNA 2′-*O*-methylation but not pseudouridylation (66). Taken together with the observation that GPATCH4 associates with box C/D snoRNAs whose target modifications are not affected by lack of the G-patch protein, this suggests that the snoRNA-interactome of GPACTH4 extends beyond the snoRNAs guiding GPATCH4-dependent RNA modifications. It is tempting to speculate that GPATCH4 may transiently associate with a large number of snoRNAs but only form functionally relevant interactions with a subset. Although we demonstrate that GPATCH4 binds RNA directly via its disordered regions, it remains unknown what features of snoRNAs/snoRNPs are specifically recognised or bound by GPATCH4, and how they contribute to its preferential association with box C/D snoRNPs.

Intriguingly, the G-patch and coiled-coil domains of GPATCH4 are separated and flanked by disordered regions. IDRs in proteins can contribute to liquid-liquid phase separation (LLPS) and often mediate interactions with RNAs (80). The GPATCH4 disordered regions are strikingly lysine-rich, making them ideally suited for forming electrostatic interaction with negatively charged RNA, and consistent with this, we observed crosslinking of specific residues within the GPATCH4 disordered regions to RNA. rDNA transcription occurs at the border of the fibrillar centre (FC) and the dense fibrillar component (DFC) of the nucleolus with nascent pre-rRNAs extending into the DFC (81). Interestingly, the box C/D snoRNP component fibrillarin has been suggested to bind to the 5′ end of the pre-rRNA transcript and self-assemble via a disordered glycine- and arginine-rich (GAR) domain, a phenomenon that has been proposed to drive phase separation of the FC and directional pre-rRNA sorting (82). Although this potential function is independent of its methyltransferase activity, it could be linked to the installation of snoRNA-guided modifications. Our ChIP and CRAC data strongly suggest that GPATCH4 also resides at the FC-DFC interface, where it may similarly contribute to coordinating pre-rRNA synthesis and modification.

The absence of GPATCH4 leads to substantial ribosome hypomethylation but it currently remains unknown what determines the dependence of a 2′-*O*-methylation on GPATCH4 or the GPATCH4-DHX15 complex. DHX15 is an RNA helicase endowed with robust unwinding activity (27,28,54,83). Our findings that the G-patch domain of GPATCH4 stimulates the ATPase activity of DHX15 and that this activity is required for efficient 2′-*O*-methylation of 18S-G644 imply a catalytic role for DHX15 in regulating rRNA 2′-*O*-methylations affected by the lack of either of these proteins. It is tempting to speculate that the unwinding activity of DHX15 is utilised at some positions to promote resolution of pre-rRNA structures allowing snoRNA access to the target site or to resolve snoRNA-pre-rRNA basepairing in a timely manner so that specific snoRNAs are released and proximal modifications can be installed (24). It is possible that 2′-*O*-methylations depending on only GPATCH4 occur in contexts without structural or kinetic constraints that necessitate the involvement of an associated RNA helicase. It has been suggested that the release of H/ACA snoRNAs from their pre-rRNA basepairing sites after pseudouridylation is a self-regulated process and it is possible that this is also the case for some C/D snoRNAs (84). It is intriguing that despite the presence of DHX15 and GPATCH4 and another DHX15-associated G-patch protein TFIP11 in Cajal

bodies, both G-patch proteins seem to influence snRNA 2′-O-methylation independently of their interactions with the helicase. Depletion of DHX15 itself does, however, impact both snRNA and rRNA 2′-O-methylation. While it is possible that the observed effects arise indirectly due to the role of the helicase in pre-mRNA splicing, the finding that rRNA 2′-O-methylation is unaffected in yeast strains lacking the key components of the splicing machinery (23) suggests that this is not the case and that the reduced snRNA and rRNA modification in cells depleted of DHX15 reflect direct roles of the helicase in ribosomal subunit and snRNP assembly.

Despite the hypomethylation of numerous rRNA nucleotides in the GPATCH4 KO cell line, pre-rRNA processing occurs as in wild-type cells and the ribosomal subunit profile of the two cell lines was similar. This suggests that the modifications installed in a GPATCH4-dependent manner are not essential for ribosomal subunit assembly. This is in line with previous observations that snoRNAs chaperoning pre-rRNA folding, such as U3 and U8 are necessary for rRNA maturation and subunit assembly while those guiding rRNA modifications are often dispensable (85,86). The absence of GPATCH4 does, however, significantly decrease the proliferation of HEK293 cells, demonstrating that it has an important cellular function. Perturbations in snRNA modification profiles are associated with defects in pre-mRNA splicing and changes in the rRNA modification landscape are linked to alterations in translation efficiency and fidelity (see for example, (87,88) (89)). Defects in mRNA maturation and/or protein synthesis therefore likely underlie the growth attenuation of cells lacking GPATCH4. Consistent with this, in GP4KO cells, we observed reduced nascent protein synthesis, indicating impaired function of the hypomethylated ribosomes produced in these cells.

Taken together, our study provides new insights into the regulation of multifunctional RNA helicases by protein cofactors and adds to the growing understanding of how the installation of RNA-guided rRNA and snRNA modifications is modulated.

Data availability

Deep sequencing data underlying this article are available in the Gene Expression Omnibus (GEO) database [http://www.ncbi.nlm.nih.gov/geo/] under the following accession Codes: GSE230431: CRAC datasets for GPATCH4-His-Flag and the His-Flag tag. GSE230432: Small RNA RIPseq datasets for GPATCH4-His-Flag and His-Flag. GSE230637: ChIP-seq datasets for GPATCH4-His-Flag and His-Flag. GSE235949: RiboMeth-seq datasets for WT, GPATCH4 KO, siNT and siDHX15. The mass spectrometry proteomics data have been deposited to the ProteomeXchange Consortium via the PRIDE partner repository [https://www.ebi.ac.uk/pride/] with the dataset identifier PXD043301.

Supplementary data

Supplementary Data are available at NAR Online.

Acknowledgements

We thank Monika Raabe and Ralf Pflanz for assistance with mass spectrometric analysis.

Funding

Deutsche Forschungsgemeinschaft (DFG) via SFB1565 [469281184; P03 to A.P., P04 to H.U., P06 to M.T.B. and P12 to K.E.B.]. Funding for open access charge: Deutsche Forschungsgemeinschaft [SFB1565 469281184].

Conflict of interest statement

None declared.

References

1. Khatter,H., Myasnikov,A.G., Natchiar,S.K. and Klaholz,B.P. (2015) Structure of the human 80S ribosome. *Nature*, **520**, 640–645.
2. Natchiar,S.K., Myasnikov,A.G., Kratzat,H., Hazemann,I. and Klaholz,B.P. (2017) Visualization of chemical modifications in the human 80S ribosome structure. *Nature*, **551**, 472–477.
3. Klinge,S. and Woolford,J.L. (2019) Ribosome assembly coming into focus. *Nat. Rev. Mol. Cell Biol.*, **20**, 116–131.
4. Bohnsack,K.E. and Bohnsack,M.T. (2019) Uncovering the assembly pathway of human ribosomes and its emerging links to disease. *EMBO J.*, **38**, e100278.
5. Dörner,K., Ruggeri,C., Zemp,I. and Kutay,U. (2023) Ribosome biogenesis factors-from names to functions. *EMBO J.*, **42**, e112699.
6. Steitz,J.A., Berg,C., Hendrick,J.P., La Branche-Chabot,H., Metspalu,A., Rinke,J. and Yario,T. (1988) A 5S rRNA/L5 complex is a precursor to ribosome assembly in mammalian cells. *J. Cell Biol.*, **106**, 545–556.
7. Zhang,J., Harnpicharnchai,P., Jakovljevic,J., Tang,L., Guo,Y., Oeffinger,M., Rout,M.P., Hiley,S.L., Hughes,T. and Woolford,J.L. (2007) Assembly factors Rpf2 and Rrs1 recruit 5S rRNA and ribosomal proteins rpL5 and rpL11 into nascent ribosomes. *Genes Dev.*, **21**, 2580–2592.
8. Schneider,C. and Bohnsack,K.E. (2022) Caught in the act-Visualizing ribonucleases during eukaryotic ribosome assembly. *Wiley Interdiscip. Rev. RNA*, **14**, e1766.
9. Matera,A.G. and Wang,Z. (2014) A day in the life of the spliceosome. *Nat. Rev. Mol. Cell Biol.*, **15**, 108–121.
10. Kunkel,G.R., Maser,R.L., Calvet,J.P. and Pederson,T. (1986) U6 small nuclear RNA is transcribed by RNA polymerase III. *Proc. Natl. Acad. Sci. U.S.A.*, **83**, 8575–8579.
11. Wang,Q., Sawyer,I.A., Sung,M.-H., Sturgill,D., Shevtsov,S.P., Pegoraro,G., Hakim,O., Baek,S., Hager,G.L. and Dundr,M. (2016) Cajal bodies are linked to genome conformation. *Nat. Commun.*, **7**, 10966.
12. Fischer,U., Englbrecht,C. and Chari,A. (2011) Biogenesis of spliceosomal small nuclear ribonucleoproteins. *Wiley Interdiscip. Rev. RNA*, **2**, 718–731.
13. Bohnsack,M.T. and Sloan,K.E. (2018) Modifications in small nuclear RNAs and their roles in spliceosome assembly and function. *Biol. Chem.*, **399**, 1265–1276.
14. Sloan,K.E., Warda,A.S., Sharma,S., Entian,K.-D., Lafontaine,D.L.J. and Bohnsack,M.T. (2017) Tuning the ribosome: the influence of rRNA modification on eukaryotic ribosome biogenesis and function. *RNA Biol.*, **14**, 1138–1152.
15. Watkins,N.J. and Bohnsack,M.T. (2012) The box C/D and H/ACA snoRNPs: key players in the modification, processing and the dynamic folding of ribosomal RNA. *Wiley Interdiscip. Rev. RNA*, **3**, 397–414.
16. Kiss-László,Z., Henry,Y., Bachellerie,J.P., Caizergues-Ferrer,M. and Kiss,T. (1996) Site-specific ribose methylation of preribosomal RNA: a novel function for small nucleolar RNAs. *Cell*, **85**, 1077–1088.
17. Ganot,P., Bortolin,M.L. and Kiss,T. (1997) Site-specific pseudouridine formation in preribosomal RNA is guided by small nucleolar RNAs. *Cell*, **89**, 799–809.

18. Sharma,S., Langhendries,J.-L., Watzinger,P., Kötter,P., Entian,K.-D. and Lafontaine,D.L.J. (2015) Yeast Kre33 and human NAT10 are conserved 18S rRNA cytosine acetyltransferases that modify tRNAs assisted by the adaptor Tan1/THUMPD1. *Nucleic Acids Res.*, **43**, 2242–2258.
19. Dutca,L.M., Gallagher,J.E.G. and Baserga,S.J. (2011) The initial U3 snoRNA:pre-rRNA base pairing interaction required for pre-18S rRNA folding revealed by in vivo chemical probing. *Nucleic Acids Res.*, **39**, 5164–5180.
20. Peculis,B.A. (1997) The sequence of the 5' end of the U8 small nucleolar RNA is critical for 5.8S and 28S rRNA maturation. *Mol. Cell. Biol.*, **17**, 3702–3713.
21. Joret,C., Capeyrou,R., Belhabich-Baumas,K., Plisson-Chastang,C., Ghandour,R., Humbert,O., Fribourg,S., Leulliot,N., Lebaron,S., Henras,A.K., *et al.* (2018) The Npa1p complex chaperones the assembly of the earliest eukaryotic large ribosomal subunit precursor. *PLoS Genet.*, **14**, e1007597.
22. Khreiss,A., Bohnsack,K.E. and Bohnsack,M.T. (2023) Molecular functions of RNA helicases during ribosomal subunit assembly. *Biol. Chem.*, **404**, 781–789.
23. Bailey,A.D., Talkish,J., Ding,H., Igel,H., Duran,A., Mantripragada,S., Paten,B. and Ares,M. (2022) Concerted modification of nucleotides at functional centers of the ribosome revealed by single-molecule RNA modification profiling. *eLife*, **11**, e76562.
24. Aquino,G.R.R., Krogh,N., Hackert,P., Martin,R., Gallesio,J.D., van Nues,R.W., Schneider,C., Watkins,N.J., Nielsen,H., Bohnsack,K.E., *et al.* (2021) RNA helicase-mediated regulation of snoRNP dynamics on pre-ribosomes and rRNA 2'-O-methylation. *Nucleic Acids Res.*, **49**, 4066–4084.
25. Bohnsack,M.T., Martin,R., Granneman,S., Ruprecht,M., Schleiff,E. and Tollervey,D. (2009) Prp43 bound at different sites on the pre-rRNA performs distinct functions in ribosome synthesis. *Mol. Cell*, **36**, 583–592.
26. Bohnsack,K.E., Kanwal,N. and Bohnsack,M.T. (2022) Prp43/DHX15 exemplify RNA helicase multifunctionality in the gene expression network. *Nucleic Acids Res.*, **50**, 9012–9022.
27. Memet,I., Doebele,C., Sloan,K.E. and Bohnsack,M.T. (2017) The G-patch protein NF-κB-repressing factor mediates the recruitment of the exonuclease XRN2 and activation of the RNA helicase DHX15 in human ribosome biogenesis. *Nucleic Acids Res.*, **45**, 5359–5374.
28. Arenas,J.E. and Abelson,J.N. (1997) Prp43: an RNA helicase-like factor involved in spliceosome disassembly. *Proc. Natl. Acad. Sci. U.S.A.*, **94**, 11798–11802.
29. Burke,J.E., Longhurst,A.D., Merkurjev,D., Sales-Lee,J., Rao,B., Moresco,J.J., Yates,J.R., Li,J.J. and Madhani,H.D. (2018) Spliceosome Profiling Visualizes Operations of a Dynamic RNP at Nucleotide Resolution. *Cell*, **173**, 1014–1030.
30. Zhang,X., Zhan,X., Yan,C., Zhang,W., Liu,D., Lei,J. and Shi,Y. (2019) Structures of the human spliceosomes before and after release of the ligated exon. *Cell Res.*, **29**, 274–285.
31. Mosallanejad,K., Sekine,Y., Ishikura-Kinoshita,S., Kumagai,K., Nagano,T., Matsuzawa,A., Takeda,K., Naguro,I. and Ichijo,H. (2014) The DEAH-box RNA helicase DHX15 activates NF-κB and MAPK signaling downstream of MAVS during antiviral responses. *Sci. Signal*, **7**, ra40.
32. Wang,P., Zhu,S., Yang,L., Cui,S., Pan,W., Jackson,R., Zheng,Y., Rongvaux,A., Sun,Q., Yang,G., *et al.* (2015) Nlrp6 regulates intestinal antiviral innate immunity. *Science*, **350**, 826–830.
33. Bohnsack,K.E., Ficner,R., Bohnsack,M.T. and Jonas,S. (2021) Regulation of DEAH-box RNA helicases by G-patch proteins. *Biol. Chem.*, **402**, 561–579.
34. Aravind,L. and Koonin,E.V. (1999) G-patch: a new conserved domain in eukaryotic RNA-processing proteins and type D retroviral polyproteins. *Trends Biochem. Sci.*, **24**, 342–344.
35. Studer,M.K., Ivanović,L., Weber,M.E., Marti,S. and Jonas,S. (2020) Structural basis for DEAH-helicase activation by G-patch proteins. *Proc. Natl. Acad. Sci. U.S.A.*, **117**, 7159–7170.
36. Hamann,F., Schmitt,A., Favretto,F., Hofele,R., Neumann,P., Xiang,S., Urlaub,H., Zweckstetter,M. and Ficner,R. (2020) Structural analysis of the intrinsically disordered splicing factor Spp2 and its binding to the DEAH-box ATPase Prp2. *Proc. Natl. Acad. Sci. U.S.A.*, **117**, 2948–2956.
37. Duchemin,A., O'Grady,T., Hanache,S., Mereau,A., Thiry,M., Wacheul,L., Michaux,C., Perpète,E., Hervouet,E., Peixoto,P., *et al.* (2021) DHX15-independent roles for TFIP11 in U6 snRNA modification, U4/U6.U5 tri-snRNP assembly and pre-mRNA splicing fidelity. *Nat. Commun.*, **12**, 6648.
38. Ran,F.A., Hsu,P.D., Wright,J., Agarwala,V., Scott,D.A. and Zhang,F. (2013) Genome engineering using the CRISPR-Cas9 system. *Nat. Protoc.*, **8**, 2281–2308.
39. Warda,A.S., Freytag,B., Haag,S., Sloan,K.E., Görlich,D. and Bohnsack,M.T. (2016) Effects of the Bowen-Conradi syndrome mutation in EMG1 on its nuclear import, stability and nucleolar recruitment. *Hum. Mol. Genet.*, **25**, 5353–5364.
40. Sloan,K.E., Leisegang,M.S., Doebele,C., Ramírez,A.S., Simm,S., Safferthal,C., Kretschmer,J., Schorge,T., Markoutsa,S., Haag,S., *et al.* (2015) The association of late-acting snoRNPs with human pre-ribosomal complexes requires the RNA helicase DDX21. *Nucleic Acids Res.*, **43**, 553–564.
41. Kiianitsa,K., Solinger,J.A. and Heyer,W.-D. (2003) NADH-coupled microplate photometric assay for kinetic studies of ATP-hydrolyzing enzymes with low and high specific activities. *Anal. Biochem.*, **321**, 266–271.
42. Haag,S., Kretschmer,J., Sloan,K.E. and Bohnsack,M.T. (2017) Crosslinking Methods to Identify RNA Methyltransferase Targets In Vivo. *Methods Mol. Biol.*, **1562**, 269–281.
43. Bohnsack,M.T., Tollervey,D. and Granneman,S. (2012) Identification of RNA helicase target sites by UV cross-linking and analysis of cDNA. *Methods Enzymol.*, **511**, 275–288.
44. Kramer,K., Sachsenberg,T., Beckmann,B.M., Qamar,S., Boon,K.-L., Hentze,M.W., Kohlbacher,O. and Urlaub,H. (2014) Photo-cross-linking and high-resolution mass spectrometry for assignment of RNA-binding sites in RNA-binding proteins. *Nat. Methods*, **11**, 1064–1070.
45. Wang,C., Ulryck,N., Herzel,L., Pythoud,N., Kleiber,N., Guérineau,V., Jactel,V., Moritz,C., Bohnsack,M.T., Carapito,C., *et al.* (2023) N 2-methylguanosine modifications on human tRNAs and snRNA U6 are important for cell proliferation, protein translation and pre-mRNA splicing. *Nucleic Acids Res.*, **51**, 7496–7519.
46. Kleiber,N., Lemus-Diaz,N., Stiller,C., Heinrichs,M., Mai,M.M.-Q., Hackert,P., Richter-Dennerlein,R., Höbartner,C., Bohnsack,K.E. and Bohnsack,M.T. (2022) The RNA methyltransferase METTL8 installs m3C32 in mitochondrial tRNAsThr/Ser(UCN) to optimise tRNA structure and mitochondrial translation. *Nat. Commun.*, **13**, 209.
47. Krogh,N., Jansson,M.D., Häfner,S.J., Tehler,D., Birkedal,U., Christensen-Dalsgaard,M., Lund,A.H. and Nielsen,H. (2016) Profiling of 2'-O-Me in human rRNA reveals a subset of fractionally modified positions and provides evidence for ribosome heterogeneity. *Nucleic Acids Res.*, **44**, 7884–7895.
48. Krogh,N. and Nielsen,H. (2019) Sequencing-based methods for detection and quantitation of ribose methylations in RNA. *Methods*, **156**, 5–15.
49. Aquino,G.R.R., Hackert,P., Krogh,N., Pan,K.-T., Jaafar,M., Henras,A.K., Nielsen,H., Urlaub,H., Bohnsack,K.E. and Bohnsack,M.T. (2021) The RNA helicase Dbp7 promotes domain V/VI compaction and stabilization of inter-domain interactions during early 60S assembly. *Nat. Commun.*, **12**, 6152.
50. Birkedal,U., Christensen-Dalsgaard,M., Krogh,N., Sabarinathan,R., Gorodkin,J. and Nielsen,H. (2015) Profiling of ribose methylations in RNA by high-throughput sequencing. *Angew. Chem. Int. Ed. Engl.*, **54**, 451–455.
51. Krogh,N., Kongsbak-Wismann,M., Geisler,C. and Nielsen,H. (2017) Substoichiometric ribose methylations in spliceosomal snRNAs. *Org. Biomol. Chem.*, **15**, 8872–8876.

52. Yu,Y.T., Shu,M.D. and Steitz,J.A. (1997) A new method for detecting sites of 2'-O-methylation in RNA molecules. *RNA*, **3**, 324–331.
53. Niu,Z., Jin,W., Zhang,L. and Li,X. (2012) Tumor suppressor RBM5 directly interacts with the DExD/H-box protein DHX15 and stimulates its helicase activity. *FEBS Lett.*, **586**, 977–983.
54. Inesta-Vaquera,F., Chaugule,V.K., Galloway,A., Chandler,L., Rojas-Fernandez,A., Weidlich,S., Peggie,M. and Cowling,V.H. (2018) DHX15 regulates CMTR1-dependent gene expression and cell proliferation. *Life Sci Alliance*, **1**, e201800092.
55. Chen,Z., Gui,B., Zhang,Y., Xie,G., Li,W., Liu,S., Xu,B., Wu,C., He,L., Yang,J., *et al.* (2017) Identification of a 35S U4/U6.U5 tri-small nuclear ribonucleoprotein (tri-snRNP) complex intermediate in spliceosome assembly. *J. Biol. Chem.*, **292**, 18113–18128.
56. Hirawake-Mogi,H., Thanh Nhan,N.T. and Okuwaki,M. (2021) G-patch domain-containing protein 4 localizes to both the nucleoli and Cajal bodies and regulates cell growth and nucleolar structure. *Biochem. Biophys. Res. Commun.*, **559**, 99–105.
57. Chen,Y.-L., Capeyrou,R., Humbert,O., Mouffok,S., Kadri,Y.A., Lebaron,S., Henras,A.K. and Henry,Y. (2014) The telomerase inhibitor Gno1p/PINX1 activates the helicase Prp43p during ribosome biogenesis. *Nucleic Acids Res.*, **42**, 7330–7345.
58. Fourmann,J.-B., Tauchert,M.J., Ficner,R., Fabrizio,P. and Lührmann,R. (2017) Regulation of Prp43-mediated disassembly of spliceosomes by its cofactors Ntr1 and Ntr2. *Nucleic Acids Res.*, **45**, 4068–4080.
59. Tsai,Y.-T., Lin,C.-I., Chen,H.-K., Lee,K.-M., Hsu,C.-Y., Yang,S.-J. and Yeh,N.-H. (2008) Chromatin tethering effects of hNopp140 are involved in the spatial organization of nucleolus and the rRNA gene transcription. *J. Biomed. Sci.*, **15**, 471–486.
60. Choudhury,P., Kretschmer,J., Hackert,P., Bohnsack,K.E. and Bohnsack,M.T. (2021) The DExD box ATPase DDX55 is recruited to domain IV of the 28S ribosomal RNA by its C-terminal region. *RNA Biol.*, **18**, 1124–1135.
61. Granneman,S., Kudla,G., Petfalski,E. and Tollervey,D. (2009) Identification of protein binding sites on U3 snoRNA and pre-rRNA by UV cross-linking and high-throughput analysis of cDNAs. *Proc. Natl. Acad. Sci. U.S.A.*, **106**, 9613–9618.
62. Manikas,R.-G., Thomson,E., Thoms,M. and Hurt,E. (2016) The K^+-dependent GTPase Nug1 is implicated in the association of the helicase Dbp10 to the immature peptidyl transferase centre during ribosome maturation. *Nucleic Acids Res.*, **44**, 1800–1812.
63. Dodel,M., Guiducci,G., Dermit,M., Krishnamurthy,S., Stojic,L. and Mardakheh,F.K. (2023) TREX reveals proteins that bind to specific RNA regions in living cells. bioRxiv doi: https://doi.org/10.1101/2023.06.30.547259, 30 June 2023, preprint: not peer reviewed.
64. Calabretta,S. and Richard,S. (2015) Emerging Roles of Disordered Sequences in RNA-Binding Proteins. *Trends Biochem. Sci.*, **40**, 662–672.
65. Meier,U.T. and Blobel,G. (1992) Nopp140 shuttles on tracks between nucleolus and cytoplasm. *Cell*, **70**, 127–138.
66. Bizarro,J., Deryusheva,S., Wacheul,L., Gupta,V., Ernst,F.G.M., Lafontaine,D.L.J., Gall,J.G. and Meier,U.T. (2021) Nopp140-chaperoned 2'-O-methylation of small nuclear RNAs in Cajal bodies ensures splicing fidelity. *Genes Dev.*, **35**, 1123–1141.
67. Warner,J.R. (1999) The economics of ribosome biosynthesis in yeast. *Trends Biochem. Sci*, **24**, 437–440.
68. Enders,M., Ficner,R. and Adio,S. (2022) Regulation of the DEAH/RHA helicase Prp43 by the G-patch factor Pfa1. *Proc. Natl. Acad. Sci. U.S.A.*, **119**, e2203567119.
69. Zhao,J., Xie,W., Yang,Z., Zhao,M., Ke,T., Xu,C., Li,H., Chen,Q. and Wang,Q.K. (2022) Identification and characterization of a special type of subnuclear structure: aGGF1-coated paraspeckles. *FASEB J.*, **36**, e22366.
70. Lin,M.-L., Fukukawa,C., Park,J.-H., Naito,K., Kijima,K., Shimo,A., Ajiro,M., Nishidate,T., Nakamura,Y. and Katagiri,T. (2009) Involvement of G-patch domain containing 2 overexpression in breast carcinogenesis. *Cancer Sci.*, **100**, 1443–1450.
71. Zhang,J., Huang,J., Xu,K., Xing,P., Huang,Y., Liu,Z., Tong,L. and Manley,J.L. (2022) DHX15 is involved in SUGP1-mediated RNA missplicing by mutant SF3B1 in cancer. *Proc. Natl. Acad. Sci. U.S.A.*, **119**, e2216712119.
72. Wen,X., Tannukit,S. and Paine,M.L. (2008) TFIP11 interacts with mDEAH9, an RNA helicase involved in spliceosome disassembly. *Int. J. Mol. Sci.*, **9**, 2105–2113.
73. De Maio,A., Yalamanchili,H.K., Adamski,C.J., Gennarino,V.A., Liu,Z., Qin,J., Jung,S.Y., Richman,R., Orr,H. and Zoghbi,H.Y. (2018) RBM17 Interacts with U2SURP and CHERP to Regulate Expression and Splicing of RNA-Processing Proteins. *Cell Rep.*, **25**, 726–736.
74. Heininger,A.U., Hackert,P., Andreou,A.Z., Boon,K.-L., Memet,I., Prior,M., Clancy,A., Schmidt,B., Urlaub,H., Schleiff,E., *et al.* (2016) Protein cofactor competition regulates the action of a multifunctional RNA helicase in different pathways. *RNA Biol.*, **13**, 320–330.
75. Feng,X., Guo,Z., Nourbakhsh,M., Hauser,H., Ganster,R., Shao,L. and Geller,D.A. (2002) Identification of a negative response element in the human inducible nitric-oxide synthase (hiNOS) promoter: the role of NF-kappa B-repressing factor (NRF) in basal repression of the hiNOS gene. *Proc. Natl. Acad. Sci. U.S.A.*, **99**, 14212–14217.
76. Nourbakhsh,M. and Hauser,H. (1999) Constitutive silencing of IFN-beta promoter is mediated by NRF (NF-kappaB-repressing factor), a nuclear inhibitor of NF-kappaB. *EMBO J.*, **18**, 6415–6425.
77. Zhou,X.Z. and Lu,K.P. (2001) The Pin2/TRF1-interacting protein PinX1 is a potent telomerase inhibitor. *Cell*, **107**, 347–359.
78. Bizarro,J., Bhardwaj,A., Smith,S. and Meier,U.T. (2019) Nopp140-mediated concentration of telomerase in Cajal bodies regulates telomere length. *Mol. Biol. Cell*, **30**, 3136–3150.
79. Chen,H.K., Pai,C.Y., Huang,J.Y. and Yeh,N.H. (1999) Human Nopp140, which interacts with RNA polymerase I: implications for rRNA gene transcription and nucleolar structural organization. *Mol. Cell. Biol.*, **19**, 8536–8546.
80. Stenström,L., Mahdessian,D., Gnann,C., Cesnik,A.J., Ouyang,W., Leonetti,M.D., Uhlén,M., Cuylen-Haering,S., Thul,P.J. and Lundberg,E. (2020) Mapping the nucleolar proteome reveals a spatiotemporal organization related to intrinsic protein disorder. *Mol. Syst. Biol.*, **16**, e9469.
81. Lafontaine,D.L.J., Riback,J.A., Bascetin,R. and Brangwynne,C.P. (2021) The nucleolus as a multiphase liquid condensate. *Nat. Rev. Mol. Cell Biol.*, **22**, 165–182.
82. Yao,R.-W., Xu,G., Wang,Y., Shan,L., Luan,P.-F., Wang,Y., Wu,M., Yang,L.-Z., Xing,Y.-H., Yang,L., *et al.* (2019) Nascent Pre-rRNA Sorting via Phase Separation Drives the Assembly of Dense Fibrillar Components in the Human Nucleolus. *Mol. Cell*, **76**, 767–783.
83. Maul-Newby,H.M., Amorello,A.N., Sharma,T., Kim,J.H., Modena,M.S., Prichard,B.E. and Jurica,M.S. (2022) A model for DHX15 mediated disassembly of A-complex spliceosomes. *RNA*, **28**, 583–595.
84. Yang,X., Duan,J., Li,S., Wang,P., Ma,S., Ye,K. and Zhao,X.S. (2012) Kinetic and thermodynamic characterization of the reaction pathway of box H/ACA RNA-guided pseudouridine formation. *Nucleic Acids Res.*, **40**, 10925–10936.
85. Esguerra,J., Warringer,J. and Blomberg,A. (2008) Functional importance of individual rRNA 2'-O-ribose methylations revealed by high-resolution phenotyping. *RNA*, **14**, 649–656.
86. Langhendries,J.-L., Nicolas,E., Doumont,G., Goldman,S. and Lafontaine,D.L.J. (2016) The human box C/D snoRNAs U3 and U8 are required for pre-rRNA processing and tumorigenesis. *Oncotarget*, **7**, 59519–59534.
87. Häfner,S.J., Jansson,M.D., Altinel,K., Andersen,K.L., Abay-Nørgaard,Z., Ménard,P., Fontenas,M., Sørensen,D.M., Gay,D.M., Arendrup,F.S., *et al.* (2023) Ribosomal RNA

2'-O-methylation dynamics impact cell fate decisions. *Dev. Cell*, **58**, 1593–1609.
88. Jansson,M.D., Häfner,S.J., Altinel,K., Tehler,D., Krogh,N., Jakobsen,E., Andersen,J.V., Andersen,K.L., Schoof,E.M., Ménard,P., *et al.* (2021) Regulation of translation by site-specific ribosomal RNA methylation. *Nat. Struct. Mol. Biol.*, **28**, 889–899.
89. Liu,L., Liu,Z., Liu,Q., Wu,W., Lin,P., Liu,X., Zhang,Y., Wang,D., Prager,B.C., Gimple,R.C., *et al.* (2023) LncRNA INHEG promotes glioma stem cell maintenance and tumorigenicity through regulating rRNA 2'-O-methylation. *Nat. Commun.*, **14**, 7526.
90. Krogh,N., Asmar,F., Côme,C., Munch-Petersen,H.F., Grønbæk,K. and Nielsen,H. (2020) Profiling of ribose methylations in ribosomal RNA from diffuse large B-cell lymphoma patients for evaluation of ribosomes as drug targets. *NAR Cancer*, **2**, zcaa035.
91. Iyer-Bierhoff,A., Krogh,N., Tessarz,P., Ruppert,T., Nielsen,H. and Grummt,I. (2018) SIRT7-dependent deacetylation of fibrillarin controls histone H2A methylation and rRNA synthesis during the cell cycle. *Cell Rep.*, **25**, 2946–2954.

Received: August 10, 2023. **Revised:** December 1, 2023. **Editorial Decision:** December 1, 2023. **Accepted:** December 5, 2023